Molecular Therapy
Methods & Clinical Development
Original Article

Modulation of the pharmacokinetics of soluble ACE2 decoy receptors through glycosylation

Savanna Skeeters,[1] Kamal Bagale,[2] Galina Stepanyuk,[1] David Thieker,[1] Aaron Aguhob,[1] Kui K. Chan,[1] Benjamin Dutzar,[1] Sergei Shalygin,[3] Asif Shajahan,[3] Xu Yang,[3] Paul A. DaRosa,[1] Emily Frazier,[1] Maximilian M. Sauer,[1] Lisa Bogatzki,[1] Kelly A. Byrnes-Blake,[4] Yifan Song,[1] Parastoo Azadi,[3] Eric Tarcha,[1] Lianghui Zhang,[2,5,6] and Erik Procko[1,7]

[1]Cyrus Biotechnology, Seattle, WA 98121, USA; [2]Division of Pulmonary, Allergy, Critical Care, and Sleep Medicine, School of Medicine, University of Pittsburgh, Pittsburgh, PA 15261, USA; [3]Complex Carbohydrate Research Center, University of Georgia, Athens, GA 30602, USA; [4]Northwest PK Solutions, Bothell, WA 98021, USA; [5]Vascular Medicine Institute, School of Medicine, University of Pittsburgh, Pittsburgh, PA 15261, USA; [6]Center for Vaccine Research, School of Medicine, University of Pittsburgh, Pittsburgh, PA 15261, USA; [7]Department of Biochemistry, University of Illinois, Urbana, IL 61801, USA

The Spike of SARS-CoV-2 recognizes a transmembrane protease, angiotensin-converting enzyme 2 (ACE2), on host cells to initiate infection. Soluble derivatives of ACE2, in which Spike affinity is enhanced and the protein is fused to Fc of an immunoglobulin, are potent decoy receptors that reduce disease in animal models of COVID-19. Mutations were introduced into an ACE2 decoy receptor, including adding custom N-glycosylation sites and a cavity-filling substitution together with Fc modifications, which increased the decoy's catalytic activity and provided small to moderate enhancements of pharmacokinetics following intravenous and subcutaneous administration in humanized FcRn mice. Most prominently, sialylation of native glycans increases exposures by orders of magnitude, and the optimized decoy is therapeutically efficacious in a mouse COVID-19 model. Ultimately, an engineered and highly sialylated decoy receptor produced using methods suitable for manufacture of representative drug substance has high exposure with a 5- to 9-day half-life. Finally, peptide epitopes at mutated sites in the decoys generally have low binding to common HLA class II alleles and the predicted immunogenicity risk is low. Overall, glycosylation is a critical molecular attribute of ACE2 decoy receptors and modifications that combine tighter blocking of Spike with enhanced pharmacokinetics elevate this class of molecules as viable drug candidates.

INTRODUCTION

Severe acute respiratory syndrome coronavirus 2 (SARS-CoV-2) is a highly transmissible respiratory virus that infects a broad range of cell types, but especially pneumocytes and mucosal epithelia of the respiratory tract.[1] The broad tropism of the virus is driven by host cell expression of its entry receptor, angiotensin-converting enzyme 2 (ACE2), as well as other accessory factors that facilitate the entry process.[1–3] ACE2 is a dimeric protease at the plasma membrane that catalyzes the turnover of vasoconstrictive and pro-inflammatory hormones.[4–6] Trimeric Spikes (S) on the viral surface bind with moderate affinity to ACE2 via a receptor-binding domain (RBD), triggering conformational changes in S that facilitate fusion of the viral envelope and host cell membrane, releasing the viral genome into the infected cell.[7]

Antibodies targeting the RBD may block ACE2 interactions or block the necessary conformational changes associated with membrane fusion.[8–10] Monoclonal anti-RBD antibodies have been developed as highly effective drugs and prophylactics for coronavirus disease 2019 (COVID-19), yet their efficacy waned against emerging SARS-CoV-2 variants of concern (VOCs).[11–15] This was especially evident with omicron sublineages that were first reported in late 2021 in southern Africa and within weeks had spread globally to become the dominant circulating variants.[16,17] Many omicron variants are now in co-circulation in what is colloquially called a "variant soup."[18]

An alternative to monoclonal antibodies is to use the extracellular domains of the ACE2 receptor as a soluble decoy.[19] Soluble decoy receptors have been explored as inhibitors of virus infection due to their perceived breadth against virus variants. Recombinant soluble ACE2 (sACE2) alone and as a catalytically inactive immunoglobulin (Ig)M Fc fusion have been evaluated in clinical trials by intravenous (i.v.) and intranasal administration, respectively[20–22]; the sACE2-IgM chimera reduced incidence of SARS-CoV-2 infection and reduced viral load when used as post-exposure prophylaxis compared with placebo.[21] However, neither of these investigational drugs have been optimized for long half-life following systemic delivery that is necessary for long-acting pre- and post-exposure prophylaxis and durable protection of immunocompromised patients in which SARS-CoV-2 replication may persist for weeks to months.[23,24] Alternatively,

Received 13 October 2023; accepted 16 July 2024;
https://doi.org/10.1016/j.omtm.2024.101301.

Correspondence: Lianghui Zhang, Division of Pulmonary, Allergy, Critical Care, and Sleep Medicine, School of Medicine, University of Pittsburgh, Pittsburgh, PA 15261, USA.
E-mail: lhzhang@pitt.edu
Correspondence: Erik Procko, Cyrus Biotechnology, Seattle, WA 98121, USA.
E-mail: erik.procko@cyrusbio.com

an engineered sACE2 decoy receptor carrying three mutations for increased affinity to S, called $sACE2_2$.v2.4, is in preclinical development and neutralizes SARS-CoV-2 at picomolar concentrations and tightly blocks S from all VOCs as well as SARS-CoV-1 and related bat coronaviruses.[15,25–27] When fused to the Fc region of IgG1 to recruit immune effector functions, $sACE2_2$.v2.4-IgG1 is highly effective both therapeutically and prophylactically in reducing disease in human ACE2 transgenic mice inoculated with lethal doses of original, gamma, or BA.1 omicron SARS-CoV-2.[15,27]

Engineered decoy receptors for SARS-CoV-2 have two potential advantages over monoclonal antibodies: (1) unrivalled breadth against SARS-related coronaviruses that can use human ACE2 as an entry receptor,[26] and (2) catalytic activity that in-and-of-itself may ameliorate COVID-19 symptoms by down-regulating angiotensin II signaling.[27–30] However, sACE2 decoys also have potential limitations. In particular, monoclonal antibodies are stable and long-lived in the human body, and their serum stability can be further extended by months using Fc modifications,[31] whereas the serum half-lives of sACE2 proteins fused to immunoglobulin Fc are shorter.[19] The reported half-lives of engineered sACE2-Fc proteins in plasma vary substantially.[15,32–36] Interpretation of the literature is complicated by differences in route of administration, choice of animal model, source of sACE2-Fc, dose, and differences in detection methods. The fusion protein may also be degraded to produce long-lived Fc fragments.[15]

Here, we explore features and modifications to $sACE2_2$.v2.4-IgG1 for improved pharmacokinetic (PK) properties. This is accomplished through (1) mutations to protect/stabilize the ACE2 collectrin-like domain, (2) mutations in the Fc moiety that promote neonatal Fc receptor (FcRn) mediated recycling, and (3), most importantly, by high sialylation of N-glycans that decorate the decoy receptor surface.

RESULTS

Low sialylation of $sACE2_2$.v2.4-IgG1 is correlated with rapid clearance *in vivo*

The reported clearance of engineered sACE2-Fc-fusion proteins administered to mice varies from hours to days.[15,35] These inconsistencies might be explained by differences in the cell lines used for sACE2-Fc expression and purification. Antibodies and Fc-fusion proteins typically have long serum half-lives due to interactions with FcRn, which reduces protein turnover *in vivo*.[31] We i.v. administered the engineered decoy $sACE2_2$.v2.4-IgG1, produced from either nonhuman ExpiCHO-S or human Expi293F cells that were transiently transfected, to transgenic mice expressing human FcRn under the control of the human promoter (B6.Cg-Fcgrt^{tm1Dcr} Tg(FCGRT)32Dcr/DcrJ or Tg32 mice). The Tg32 mouse model more closely represents the expected PK of Fc-fusion proteins in humans.[37] Protein produced in ExpiCHO-S cells was rapidly cleared, with ACE2 catalytic activity in plasma falling to levels close to background within 2 h (Figure 1A). However, after i.v. administration of $sACE2_2$.v2.4-IgG1 from Expi293F culture, plasma ACE2 activity rapidly fell during the initial distribution phase for the first hour but then remained elevated during a slower elimination phase (Figure 1A). At time points after 4 h, catalytic activity in plasma of $sACE2_2$.v2.4-IgG1 from Expi293F cells was ∼50-fold higher compared with protein produced from ExpiCHO-S culture. These findings were confirmed by an ELISA optimized for detecting complete protein, in which the human IgG1 Fc moiety was captured on the assay plate surface and the sACE2 moiety detected with polyclonal antibody (Figure 1B). At 4 h post-administration, plasma levels of Expi293F-produced $sACE2_2$.v2.4-IgG1 were ∼9 μg/mL, whereas ExpiCHO-S-produced protein levels had rapidly fallen and were at ∼0.2 μg/mL.

Because $sACE2_2$.v2.4-IgG1 produced in the two transiently transfected cell lines is expected to have identical amino acid sequence, we reasoned that the different properties *in vivo* are due to changes in glycosylation. Glycomics analysis using mass spectrometry methods (Figures 1C, S1, and S2) revealed that N-glycans of $sACE2_2$.v2.4-IgG1 produced in ExpiCHO-S cells are 5.5-fold less sialylated than on protein from Expi293F cells (Figure 1D). Furthermore, O-glycans at Thr730 of ExpiCHO-S produced $sACE2_2$.v2.4-IgG1 are almost exclusively monosialylated core 1 structures (Figure 1E), whereas O-glycans decorating protein from Expi293F cells are more complex and 80% disialylated (Figure 1F). High sialylation is thus correlated with extended activity of $sACE2_2$.v2.4-IgG1 *in vivo*, possibly due to clearance of low sialylated protein via asialoglycoprotein receptors.[38] For the purposes of this study, we continued engineering $sACE2_2$.v2.4-IgG1 for improved PK using protein expressed in Expi293F cells to ensure high sialylation.

A derivative of $sACE2_2$.v2.4-IgG1 with increased glycosylation has higher catalytic activity *in vitro* and *in vivo*

From the N to C terminus, the ACE2 polypeptide consists of a cleaved signal peptide (amino acids, a.a., 1–17), a Zn^{2+}-dependent protease domain (a.a. 18–615), a collectrin-like domain (CLD; a.a. 616–732) that mediates dimerization, and a transmembrane helix and cytoplasmic tail (a.a. 741–805).[39] The RBD of SARS-CoV-2 physically contacts the protease domain.[39,40] Even though the CLD does not contribute direct contacts to the RBD, sACE2 proteins containing the CLD display approximately 5-fold tighter monovalent affinity, in addition to enjoying the benefits of engaging multiple S proteins avidly for enhanced neutralization potency.[19,25,41,42] The CLD has also been reported to increase the PK of soluble ACE2 constructs *in vivo*.[43] The engineered decoy receptor $sACE2_2$.v2.4-IgG1 encompasses human ACE2 residues 18–732 and is a stable dimer in both the ACE2 and IgG1 Fc moieties. $sACE2_2$.v2.4-IgG1 has three mutations (T27Y, L79T, and N330Y) that increase affinity for S by one to two orders of magnitude.[25] While the CLD enhances S binding affinity, avidity, and neutralization activity, it is also cleaved by endogenous proteases, including ADAM17, TMPRSS2, and HAT.[44] The proteolytic release of sACE2 from the plasma membrane is massively elevated during SARS-CoV-2 infection and serum sACE2 levels strongly correlate with COVID-19 severity.[45–49] Due to cleavage within the CLD, serum sACE2 released during infection is likely monomeric with low S affinity and avidity, and possibly also with

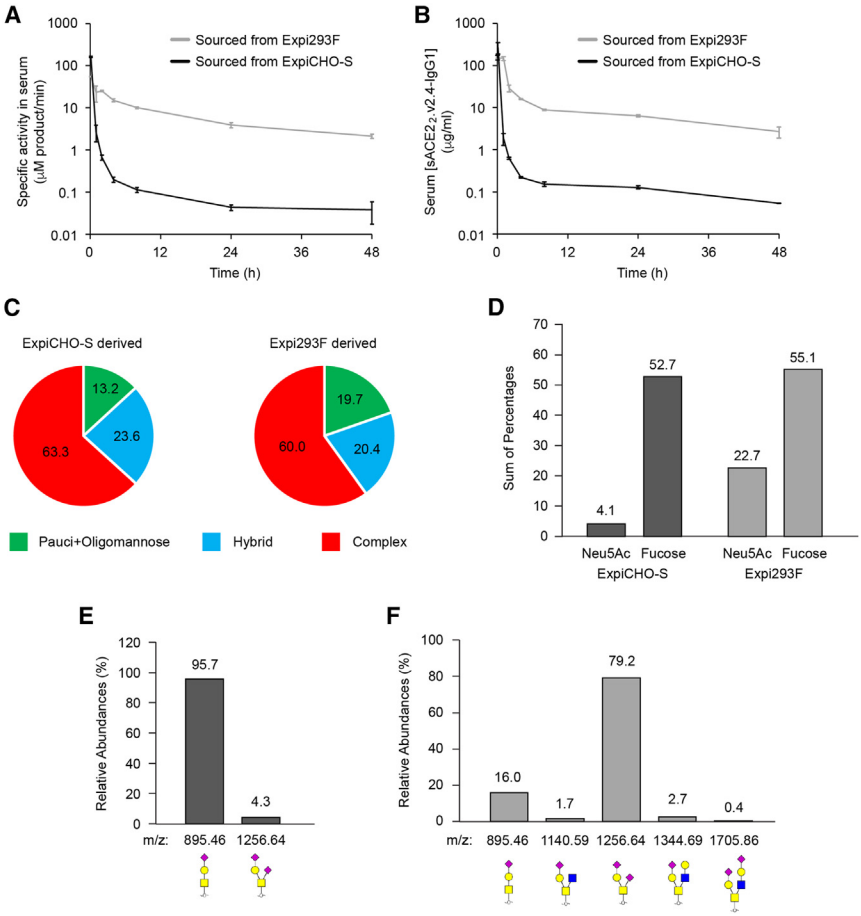

Figure 1. Choice of cell line for sACE2$_2$.v2.4-IgG1 production impacts pharmacokinetics and glycosylation

(A and B) sACE2$_2$.v2.4-IgG1 was expressed and purified from human Expi293F (gray) or nonhuman ExpiCHO-S (black) cultures that were both transiently transfected. A 10 mg/kg amount of sACE2$_2$.v2.4-IgG1 was injected into the tail vein of human FcRn transgenic mice. (A) ACE2 catalytic activity and (B) protein concentrations based on ELISA were measured in plasma. Data are mean ± SEM, n = 3 mice per time point. (C) N-glycan types from glycomics analysis of sACE2$_2$.v2.4-IgG1 produced in ExpiCHO-S vs. Expi293F cells. (D) Abundance of sialylated (Neu5Ac) and fucosylated N-glycan structures. (E and F) O-Glycan analysis of sACE2$_2$.v2.4-IgG1 produced in (E) ExpiCHO-S and (F) Expi293F cells. After PNGaseF treatment of protein, O-glycans were released, purified, permethylated, and analyzed by MALDI-TOF-MS. O-glycan structures were assigned using Glycoworkbench software based on precursor masses and the common mammalian biosynthetic pathway. Glycan structures are indicated on the x axis by their m/z ratio. GlcNAc, blue squares; GalNAc, yellow squares; Gal, yellow circles; Neu5Ac, purple diamonds.

reduced catalytic activity, supported by decreased angiotensin 1–7 (Ang(1–7); a product of ACE2 catalysis) in COVID-19 patients.[50,51] We hypothesized that protecting the CLD of sACE2$_2$.v2.4-IgG1 will enhance *in vivo* characteristics.

Three design strategies were explored (Figure 2A). First, we compared human and mouse ACE2 sequences to identify polymorphic residues. Mouse sACE2 fused to murine IgG1 Fc has a long plasma half-life (elimination phase $t_{1/2\beta}$) of 174 h following i.v. administration.[35] Polymorphic residues were selected for computational saturation mutagenesis and modeling using Rosetta software.[52] Multiple mutations were identified that decrease the computed ΔG for folding (i.e., are predicted to stabilize the structure). Our attention was drawn to cavity-filling mutations enriched at the interface between the protease domain and CLD, suggesting to us that this region is under-packed in human ACE2. Second, residue pairs were identified that when mutated to cysteine have a high probability of oxidizing to form disulfides that will constrain conformational dynamics. Seven designs with predicted stabilizing point substitutions (two to three mutations per design) and three designs with engineered disulfides were expressed and purified (Table S1).

The third design strategy was to shield sACE2$_2$.v2.4-IgG1 from proteases by introduction of N-glycosylation sites. Borrowing from the murine ACE2 sequence (which has two additional N-glycosylation motifs compared to human ACE2), as well as modeling the introduction of custom N-glycosylation motifs (Asn-X-Ser/Thr, where X is any amino acid other than proline), seven derivatives of sACE2$_2$.v2.4-IgG1 were designed with one to three added glycosylation motifs. Finally, two sACE2$_2$.v2.4-IgG1 proteins were designed that mix features of the different design strategies.

Of the 19 derivatives of sACE2$_2$.v2.4-IgG1 (the parental sequence), 15 were secreted at high levels in transiently transfected Expi293F culture and were purified. While the designs were all catalytically active, those with cavity-filling mutations tended to have reduced proteolytic activity (Figure S3). A subset of three designed proteins ("Stability/S" designs S14, S15, and S19), which shared mutations M662T and N720S to add N-glycans at residues 660 and 718 in the CLD, were found to have higher catalytic activity. This subset of sACE2$_2$.v2.4-IgG1 derivatives were also among the tighter binders to the RBD of the delta SARS-CoV-2 variant, as determined by biolayer interferometry (BLI) under conditions that measure monovalent affinity (Table 1).

The proteins were administered i.v. at 2 mg/kg to human FcRn mice and catalytic activity in plasma was measured (Figure S4A). The half-life (calculated as a combination of distribution phase $t_{1/2\alpha}$ and elimination phase $t_{1/2\beta}$) of parental sACE2$_2$.v2.4-IgG1

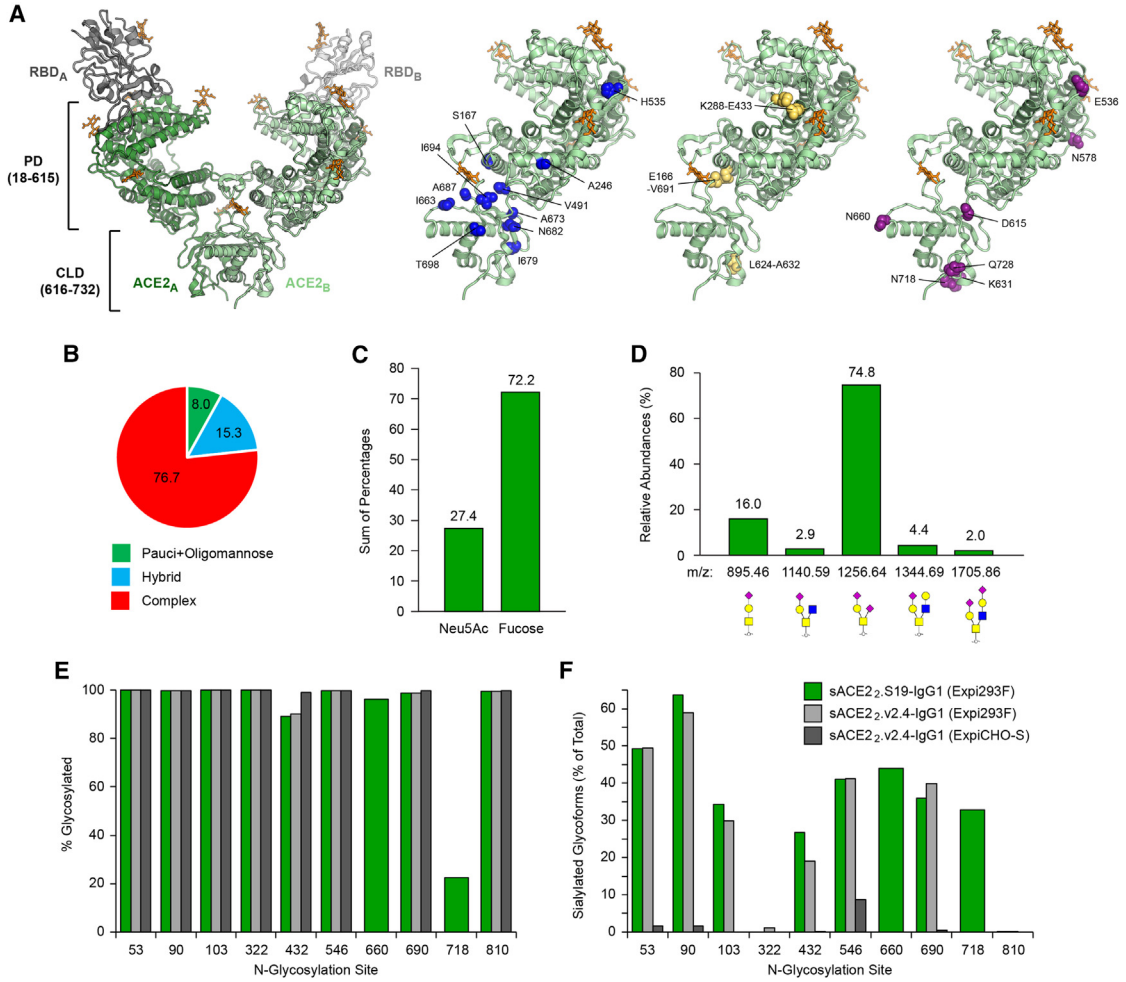

Figure 2. An engineered derivative of sACE2$_2$.v2.4-IgG1 and its glycosylation

(A) Left, the structure (PDB: 6M17) of dimeric ACE2 (chains "A" and "B" in dark and light green) bound to RBD (gray ribbons). Glycans are shown as orange sticks. PD, protease domain; CLD, collectrin-like dimerization domain. Center and right, residues mutated to fill cavities (blue spheres), introduce disulfides (yellow spheres), or add N-glycosylation motifs (purple spheres) are shown on a single ACE2 subunit. Lead candidate sACE2$_2$.S19-IgG1 has mutations V491I, M662T, N720S. (B) N-glycan types on sACE2$_2$.S19-IgG1 produced in Expi293F cells. (C) Abundance of sialylated and fucosylated N-glycan structures on sACE2$_2$.S19-IgG1 produced in Expi293F cells. (D) O-Glycan structures on sACE2$_2$.S19-IgG1 produced in Expi293F cells following O-glycan release and MALDI-TOF-MS analysis. (E) Occupancy of the N-glycosylation sites based on glycopeptidomics analysis of sACE2$_2$.S19-IgG1 from Expi293F (green), sACE2$_2$.v2.4-IgG1 from Expi293F (pale gray), and sACE2$_2$.v2.4-IgG1 from ExpiCHO-S (dark gray). sACE2$_2$.S19-IgG1 has added glycosylation sites at positions 660 and 718. (F) Percent of the glycoforms at each N-glycosylation site that have at least one sialic acid.

was 15.3 h and the area under the curve (AUC_{0-48h}) was 68.9 (μM product/minute) × h. Derivatives with cavity-filling mutations tended to have faster clearance, while derivatives with added glycosylation motifs were generally similar to the parental protein. However, the subset of derivatives S14, S15, and S19 had higher activity in plasma, consistent with their higher activity *in vitro*. Full-length protein was detected by immunoblot analysis of plasma from a single mouse administered sACE2$_2$.S14-IgG1 as a representative example (Figure S4B). The most active protein in mice, sACE2$_2$.S19-IgG1, had $t_{1/2}$ = 21.0 h and AUC_{0-48h} = 137 (μM product/minute) × h. Melting temperatures measured by differential scanning fluorimetry (DSF) are equivalent between the parental construct sACE2$_2$.v2.4-IgG1 and the derivative sACE2$_2$.S19-IgG1 (Figure S5). Our data do not discriminate between multiple possibilities for the mechanism of moderately enhanced *in vivo* stability of sACE2$_2$.S19-IgG1, which we hypothesize is mediated by glycans that block protease-sensitive sites and/or by structural stabilization of local features in the CLD.

Glycomics analysis indicated that sACE2$_2$.S19-IgG1, expressed and purified from Expi293F culture, was highly sialylated and similar to parental sACE2$_2$.v2.4-IgG1 (Figures S6 and 2B–2D). We further analyzed the sACE2$_2$.S19-IgG1 from Expi293F culture using glycopeptidomics and compared with the parental sACE2$_2$.v2.4-IgG1

Table 1. BLI kinetics for monovalent binding of decoy receptors to Spike RBD

Immobilized protein[a]	Source	Analyte	K_D (nM)	k_{on} ($M^{-1}s^{-1}$)	k_{off} (s^{-1})	χ^{2} [b]	R^{2} [b]
$sACE2_2$.S01-IgG1	Expi293F	Delta-RBD	1.0	8.7×10^5	8.4×10^{-4}	0.016	0.998
$sACE2_2$.S02-IgG1	Expi293F	Delta-RBD	1.1	8.2×10^5	9.2×10^{-4}	0.015	0.998
$sACE2_2$.S03-IgG1	Expi293F	Delta-RBD	1.3	8.8×10^5	1.2×10^{-3}	0.021	0.996
$sACE2_2$.S04-IgG1	Expi293F	Delta-RBD	1.4	8.3×10^5	1.2×10^{-3}	0.030	0.994
$sACE2_2$.S06-IgG1	Expi293F	Delta-RBD	1.6	8.6×10^5	1.4×10^{-3}	0.032	0.994
$sACE2_2$.S09-IgG1	Expi293F	Delta-RBD	1.4	8.6×10^5	1.2×10^{-3}	0.028	0.994
$sACE2_2$.S11-IgG1	Expi293F	Delta-RBD	0.9	8.8×10^5	8.2×10^{-4}	0.010	0.998
$sACE2_2$.S12-IgG1	Expi293F	Delta-RBD	1.1	9.3×10^5	1.0×10^{-3}	0.011	0.997
$sACE2_2$.S13-IgG1	Expi293F	Delta-RBD	0.9	9.9×10^5	8.7×10^{-4}	0.009	0.997
$sACE2_2$.S14-IgG1	Expi293F	Delta-RBD	0.9	9.2×10^5	8.7×10^{-4}	0.014	0.994
$sACE2_2$.S15-IgG1	Expi293F	Delta-RBD	0.8	9.3×10^5	7.3×10^{-4}	0.012	0.997
$sACE2_2$.S16-IgG1	Expi293F	Delta-RBD	0.9	9.3×10^5	8.4×10^{-4}	0.009	0.995
$sACE2_2$.S17-IgG1	Expi293F	Delta-RBD	0.7	9.8×10^5	6.9×10^{-4}	0.010	0.997
$sACE2_2$.S18-IgG1	Expi293F	Delta-RBD	0.8	9.0×10^5	7.6×10^{-4}	0.017	0.996
$sACE2_2$.S19-IgG1	Expi293F	Delta-RBD	0.6	9.3×10^5	5.8×10^{-4}	0.016	0.996
$sACE2_2$.v2.4-IgG1(YTE)	Expi293F	Wuhan-RBD	0.9	6.8×10^5	6.2×10^{-4}	0.181	0.993
$sACE2_2$.v2.4-IgG1(YTE)	Expi293F	Delta-RBD	0.4	8.7×10^5	3.6×10^{-4}	0.142	0.994
$sACE2_2$.v2.4-IgG1(YTE)	Expi293F	Gamma-RBD	0.6	9.6×10^5	5.7×10^{-4}	0.132	0.992
RD mutant	Expi293F	Wuhan-RBD	91	6.7×10^5	6.1×10^{-2}	0.074	0.960
RD mutant	Expi293F	Delta-RBD	>1000	$< 10^4$	0.14	0.078	0.935
RD mutant	Expi293F	Gamma-RBD	83	6.1×10^5	5.0×10^{-2}	0.110	0.920
$sACE2_2$.v2.4-IgG1(YTE)	CHOK1SV GS-KO	Delta-RBD	0.6	7.6×10^5	4.9×10^{-4}	0.415	0.991
$sACE2_2$.v2.4-IgG1(YTE)	CHOK1SV GS-KO	Gamma-RBD	0.8	8.2×10^5	6.6×10^{-4}	0.387	0.991
$sACE2_2$.S19-IgG1(YTE)	CHOK1SV GS-KO	Delta-RBD	0.7	7.9×10^5	5.3×10^{-4}	0.390	0.992
$sACE2_2$.S19-IgG1(YTE)	CHOK1SV GS-KO	Gamma-RBD	0.8	8.6×10^5	7.1×10^{-4}	0.397	0.991

[a]Dimeric $sACE2_2$-IgG1 proteins were immobilized to anti-human IgG sensors. Sensors were transferred to monomeric RBD-8h solutions at 90, 30, and 10 nM. Samples from Expi293F culture were tested once. Samples from CHOK1SV GS-KO culture were tested in duplicate.
[b]χ^2 and R^2 were determined from curves fitted to the data, including duplicates where relevant.

protein from Expi293F and ExpiCHO-S cell expression. This analysis provided quantitative determination of the glycoforms present at individual N-glycosylated sites (Tables S2–S11). We found that all the native N-glycosylation sites had close to 100% glycan occupancy except for N432, which was 90% glycosylated in protein from Expi293F cells and 99% glycosylated in $sACE2_2$.v2.4-IgG1 from ExpiCHO-S (Figure 2E). Of the two custom N-glycosylation motifs added to $sACE2_2$.S19-IgG1, position 660 was 96% glycosylated but position 718 was only 23% glycosylated (Figure 2E), for reasons that are unclear. The glycoforms present at each site are highly heterogeneous (Tables S2–S11). For the proteins produced in Expi293F culture, ~20%–60% of the glycoforms contained at least one sialic acid, with the exceptions of N322 and N810 (equivalent to N297 of IgG1 Fc using EU numbering) where sialylation was absent (Figure 2F). Sialylated glycans had very low relative abundance (<2%) at all positions in ExpiCHO-S produced $sACE2_2$.v2.4-IgG1, although it was moderately higher (8.7%) at position N546. Glycopeptidomics analysis thus further emphasizes that sialylation is highly dependent on the expressing cell line.

The O-glycosylation site at T730[53] was poorly glycosylated in the proteins derived from Expi293F culture (2.3%–5.0% glycosylated) and from ExpiCHO-S culture (11.1%) (Table S12). This differs from a previous report in which T730 was found to be 97% glycosylated[53] and may reflect differences in expression systems, construct length, and fusion to IgG1 (here, $sACE2_2$.v2.4-IgG1 and $sACE2_2$.S19-IgG1 are fused at residue G732 to IgG1 Fc, thus changing the environment around T730).

In summary, modifications primarily focused on stabilizing the CLD achieved higher exposure to ACE2 catalytic activity. ACE2 catalysis contributes to therapeutic efficacy in animal models of COVID-19.[27,28,30,54]

YTE mutations in the Fc moiety of the decoy receptor improve pharmacokinetics

We next considered modifying the Fc moiety of the decoy receptor based on mutations that extend the half-lives of antibodies. Substitutions M252Y, S254T, and T256E (EU numbering; referred to as YTE

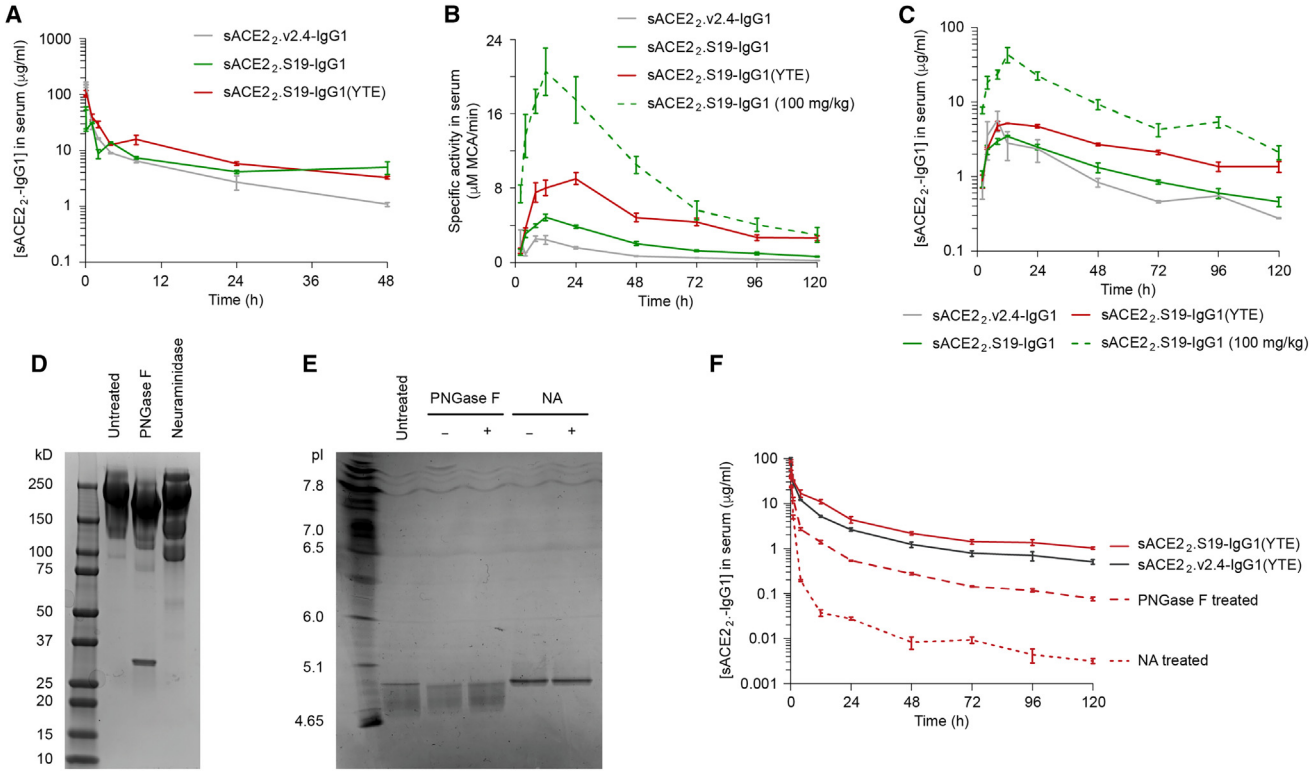

Figure 3. High sialylation and YTE mutations in the Fc region enhance the pharmacokinetics of sACE2$_2$.S19-IgG1

(A) Intravenous administration of proteins at 10 mg/kg into human FcRn mice. Blood was collected into heparin via retroorbital route at the plotted time points. Plasma levels of the indicated proteins were measured by ELISA. (B and C) Proteins were injected s.c. in the flank of human FcRn mice at a dose of 10 mg/kg (solid lines) or 100 mg/kg (broken line). (B) ACE2 catalytic activity in plasma and (C) protein concentrations based on ELISA. (D) sACE2$_2$.S19-IgG1(YTE) was treated with PNGase F or neuraminidase. Proteins (20 μg) were analyzed without further purification by SDS-PAGE under non-reducing conditions and stained with Coomassie. The calculated molecular weight (MW) of the mature polypeptide (excluding glycans) is 218 kD for the dimer. PNGase F has an MW of 36 kD. *A. ureafaciens* neuraminidase is a mixture of isoenzymes. (E) Proteins (10 μg) were analyzed by IEF gel electrophoresis. Glycosidase-treated proteins were analyzed without (–) and with (+) purification by gel filtration following treatment. (F) Purified proteins were injected i.v. at 10 mg/kg into human FcRN mice and concentrations in plasma were measured by ELISA for 5 days. For PK studies in this figure, data are mean ± SEM for $n = 3$ per group and proteins were purified from transiently transfected Expi293F.

mutations) in human IgG1 decrease the dissociation rate between Fc and FcRn 10-fold at endosomal pH, leading to a 2- to 5-fold increase in serum half-lives of antibodies.[55–57] The YTE mutations are incorporated into tixagevimab and cilgavimab, two anti-SARS-CoV-2 monoclonal antibodies that were approved for use as a combination for the prevention of COVID-19.[58] The YTE mutations also diminish antibody-dependent cell-mediated cytotoxicity and increase distribution into the lungs.[57] These properties might increase safety and efficacy of sACE2 proteins fused to IgG1 Fc.

We confirmed that the YTE mutations enhanced the affinities of sACE2$_2$.v2.4-IgG1 and sACE2$_2$.S19-IgG1 for FcRn using BLI (Figure S7). FcRn binding at pH 6.0 was tighter than at pH 7.4, reflecting the biological role of FcRn to capture internalized IgG in the acidic endosome and recycle it to the cell surface for release. We estimate that in the absence of the YTE mutations, the dissociation constants were >100 nM (accurate fitting of kinetic rate constants was not possible for these samples due to incomplete dissociation of the analyte). By comparison, sACE2$_2$.v2.4-IgG1(YTE) and sACE2$_2$.S19-IgG1(YTE) had dissociation constants for FcRn at pH 6.0 of 21 nM and 39 nM, respectively, with slow off rates of 5.9×10^{-4} s^{-1} and 1.2×10^{-3} s^{-1}.

We administered 10 mg/kg sACE2$_2$.v2.4-IgG1 and sACE2$_2$.S19-IgG1 with and without YTE mutations to human FcRn transgenic mice intravenously and measured plasma protein concentrations by ELISA (Figure 3A). sACE2$_2$.S19-IgG1(YTE) had the highest exposure (AUC_{0-48h} = 490 μg/mL × h), followed by sACE2$_2$.S19-IgG1 (310 μg/mL × h) and sACE2$_2$.v2.4-IgG1 (290 μg/mL × h). We further explored administration via the subcutaneous (s.c.) route; the serum half-lives of the decoys delivered by the s.c. route may be altered by absorption from the injection site. Based on catalytic activity in plasma (Figure 3B), adding the YTE mutations to sACE2$_2$.S19-IgG1 increased $t_{1/2}$ by an extra 11 h and exposure to ACE2 activity by 3-fold. Using ELISA to measure plasma concentrations (Figure 3C), $t_{1/2}$ of sACE2$_2$.S19-IgG1(YTE) was 51.1 h and AUC_{0-120h} was 320 μg/mL × h. Exposures were less for sACE2$_2$.S19-IgG1 (160 μg/mL × h) and sACE2$_2$.v2.4-IgG1 (150 μg/mL × h). Protein

Table 2. Pharmacokinetic properties of optimized decoy receptors in Tg32 mice

Proteins produced by transiently transfected Expi293F[a]				
$sACE2_2$-IgG1 protein	Enzyme treatment	$t_{1/2\beta}$[b] (h)	AUC_{0-120h} (μg/mL × h)	$MRT_{0\text{-inf obs}}$[c] (h)
$sACE2_2$.v2.4-IgG1(YTE)	None	60.1	330	43.4
$sACE2_2$.S19-IgG1(YTE)	None	73.0	510	60.8
$sACE2_2$.S19-IgG1(YTE)	NA/sialidase	30.8	48	2.1
Proteins produced by stable CHOK1SV GS-KO: 8-day study[a]				
$sACE2_2$-IgG1 protein	$t_{1/2\beta}$[b] (h)	AUC_{0-192h} (μg/mL × h)	$MRT_{0\text{-inf obs}}$ (h)	C_{192h} (μg/mL)[c]
$sACE2_2$.v2.4-IgG1(YTE)	124	4100	160	10 ± 2
$sACE2_2$.S19-IgG1(YTE)	224	6400	312	23 ± 3
$sACE2_2$.S19-IgG1(YTE) produced by stable CHOK1SV GS-KO: 14-day study[d]				
Route of administration	$t_{1/2\beta}$[b] (h)	AUC_{0-336h} (μg/mL × h)	$MRT_{0\text{-inf obs}}$ (h)	C_{336h} (μg/mL)[c]
i.v.	122	8540	168	9 ± 1
s.c.	196	6170	263	8 ± 2

[a]Proteins were administered as a single i.v. dose (10 mg/kg) to Tg32 mice. Plasma concentrations were measured by ELISA for 120 h (Expi293F protein) or 192 h (CHOK1SV GS-KO protein).
[b]Beta half-life is determined from 24 to 120 h (Expi293F protein) or 24–192 h (CHOK1SV GS-KO protein).
[c]MRT, mean residence time.
[d]$sACE2_2$.S19-IgG1(YTE) was administered as a single i.v. or s.c. dose (10 mg/kg) to Tg32 mice. Plasma concentrations were measured by ELISA for 336 h.

concentrations remained above the IC90 for virus neutralization[15,25,27] at 120 h post-administration (Figure 3C).

The glycoforms were manipulated on $sACE2_2$.S19-IgG1(YTE) through the action of glycosidases. PNGase F cleaves the amide linkage between asparagine and the innermost N-acetylglucosamine, releasing the entire glycan. After incubation of $sACE2_2$.S19-IgG1(YTE) from Expi293F cells with PNGase F under native conditions, the protein had increased electrophoretic mobility consistent with removal of large glycans (Figure 3D). Multiple charged species of the protein were still observed on an isoelectric focusing (IEF) gel (Figure 3E), suggesting heterogeneous sialylated glycans remained and deglycosylation was incomplete, perhaps due to inaccessibility of one or more glycosylated asparagines. Treatment of $sACE2_2$.S19-IgG1(YTE) from Expi293F culture with *Arthrobacter ureafaciens* neuraminidase (an enzyme that removes all terminal sialic acids) did not change electrophoretic mobility on a standard denaturing gel but did reduce heterogeneity on an IEF gel, as expected for removal of charged sialic acids (Figures 3D and 3E).

The pharmacokinetics of the deglycosylated proteins were compared with untreated $sACE2_2$.S19-IgG1(YTE) and $sACE2_2$.v2.4-IgG1(YTE) (Figure 3F; Table 2). Human FcRn transgenic mice were given a single i.v. dose of 10 mg/kg and concentrations in plasma were measured over 5 days. At later days, the concentrations of the untreated decoy receptors closely aligned with those observed following s.c. administration. The elimination phase $t_{1/2\beta}$ values were 73 and 60 h for $sACE2_2$.S19-IgG1(YTE) and $sACE2_2$.v2.4-IgG1(YTE), respectively, and exposures (AUC_{0-120h}) were 510 and 330 μg/mL × h. Exposure was decreased following PNGase F treatment of $sACE2_2$.S19-IgG1(YTE) but the most dramatic effect was seen following treatment with neuraminidase. Desialylated $sACE2_2$.S19-IgG1(YTE) was rapidly cleared and its exposure was decreased by two orders of magnitude. Sialylation of the decoy receptor is thus necessary for optimal pharmacokinetics.

A single delivery of $sACE2_2$.S19-IgG1(YTE) effectively enhances survival of mice infected with SARS-CoV-2

Previously, $sACE2_2$.v2.4-IgG1 has been shown to be therapeutically effective when administered via inhalation or i.v. to K18-hACE2 transgenic mice inoculated with SARS-CoV-2 variants.[15,27] However, the protein in these previous studies was purified from ExpiCHO-S culture and multiple doses were administered to overcome poor PK. We hypothesized that the PK of $sACE2_2$.S19-IgG1(YTE), produced with high sialylation from Expi293F cells, would protect SARS-CoV-2 infected animals treated with a single dose. K18-hACE2 mice were intranasally inoculated with an original variant of SARS-CoV-2 (2019n-CoV/USA_WA1/2020), which causes lethal disease and lung pathology that resembles COVID-19. Infected mice were treated 24 h later with 10 mg/kg $sACE2_2$.S19-IgG1(YTE) or IgG1 control via i.v. route. In the control group, 80% of mice died by days 6–8 post-inoculation (Figure 4A) and weight loss began at days 5 (Figure 4B). By comparison, treatment with a single dose of $sACE2_2$.S19-IgG1(YTE) delayed the start of weight loss by 1 day and reduced mortality to 30% by day 14, when mouse weights were recovering (Figures 4A and 4B). Transcript levels of viral genes in the lungs measured by quantitative PCR (qPCR) at day 7 were also reduced following treatment (Figures 4C and 4D). Therapeutic efficacy at a single i.v. dose was therefore achieved through high sialylation combined with sequence optimization of the decoy receptor.

We have previously shown that knocking out catalytic activity of the decoy receptor reduces efficacy when given as a therapeutic dose via i.v. or inhalation to K18-hACE2 mice inoculated with SARS-CoV-2

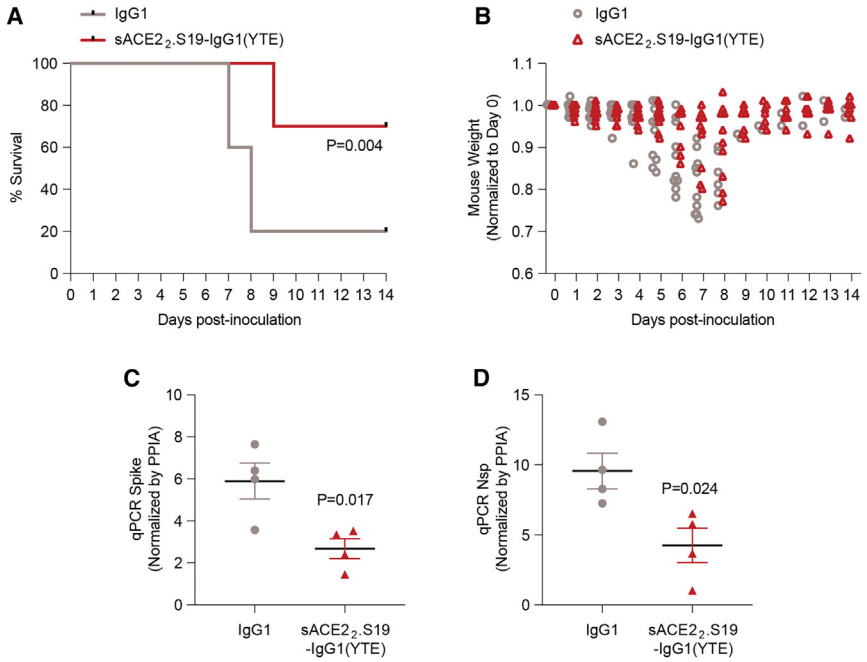

Figure 4. A single dose of sACE2$_2$.S19-IgG1(YTE) sourced from Expi293F culture protects K18-hACE2 mice from lethal SARS-CoV-2 challenge

(A and B) K18-hACE2 mice were inoculated intranasally with 1 × 10^4 PFU 2019n-CoV/USA_WA1/2020 virus. Mice were administered a single i.v. dose (10 mg/kg) of sACE2$_2$.S19-IgG1(YTE) (red; purified from transiently transfected Expi293F culture) or IgG1 control (gray) 24 h post-inoculation. Survival (A) and weights (B) for N = 10 mice per treatment group. p value determined by Gehan-Breslow-Wilcoxon test. (C and D) Lungs of inoculated mice were harvested at day 7 and relative viral loads were determined by qPCR for mRNA expression levels of SARS-CoV-2 Spike (C) and Nsp (D). Mean ± SEM, N = 4 per treatment group. p values determined by unpaired t test.

variants.[27] Here, we further demonstrate that sACE2$_2$.S19-IgG1(YTE) carrying two mutations that knock out catalytic activity (H374N and H378N,[59] referred to as the NN mutant) has partially reduced efficacy, with death beginning 2 days earlier compared with animals treated with catalytically active protein and mortality increasing to 40% (Figures S8A and S8B). However, following i.v. administration at 10 mg/kg in uninfected K18-hACE2 mice, sACE2$_2$.S19-IgG1(YTE) had $t_{1/2}$ = 27 h and AUC_{0-240h} = 590 μg/mL × h, which decreased for the NN mutant to $t_{1/2}$ = 18 h and AUC_{0-240h} = 380 μg/mL × h (Figure S8C). We conclude that the catalytically active protein has superior PK and efficacy, but we are unable to determine whether this is due to catalytic activity per se or due to indirect effects of mutations at the catalytic site that decrease plasma stability.

Decoy receptors from stable pooled expression in CHOK1SV GS-KO cells

Biologic drugs are generally purified from CHO expression systems that have well-described safety characteristics and for which there is extensive clinical experience.[60] CHOK1SV GS-KO is a suspension-adapted CHO line in which glutamine synthetase has been knocked out to facilitate methionine sulfoximine-based selection of stable clones.[61,62] A transposase integrates the gene of interest into genetically stable and high expressing genomic regions[63] and this industrially relevant cell line has been reported to yield glycoproteins with high sialylation.[64] To assess the feasibility of stable CHO expression for the manufacture of sialylated sACE2 decoy receptors, CHOK1SV GS-KO stable pools were generated for the production of sACE2$_2$.v2.4-IgG1(YTE) and sACE2$_2$.S19-IgG1(YTE). Based on capillary electrophoresis, decoy receptors purified from stable CHOK1SV GS-KO culture had equivalent purity to those from transiently transfected Expi293F cells (Figure S9A) but had sharper peaks with lower isoelectric points (pI) under isoelectric focusing (Figures S9B–S9E), suggesting reduced glycoform heterogeneity with high levels of negatively charged sugars. Sialic acids were released by acid hydrolysis and reacted to form a fluorescent product that was quantified by reverse-phase high-performance liquid chromatography (RP-HPLC). Decoy receptors from CHOK1SV GS-KO stable pools had twice the molar content of N-acetylneuraminic acid (Neu5Ac) than proteins transiently expressed by Expi293F (Table 3). Levels of N-glycolylneuraminic acid (Neu5Gc), a sialic acid that is not produced by human cells and has immunogenic potential,[65] were low (Table 3). Furthermore, decoy receptors from CHOK1SV GS-KO stable pools tightly bound the RBDs of gamma and delta SARS-CoV-2 variants with monovalent binding affinities equivalent to proteins with less sialylation from Expi293F culture (Figure S10; Table 1). We conclude that a stable CHO expression system is suitable for producing decoy receptors with high levels of sialylated N-glycans and potent affinity for virus spikes.

sACE2$_2$.v2.4-IgG1(YTE) and sACE2$_2$.S19-IgG1(YTE) from CHOK1SV GS-KO stable pooled expression were administered i.v. to human FcRn mice at a single 10 mg/kg dose and plasma exposures were measured over 8 days. The highly sialylated decoy receptors had superior PK, with plasma concentrations remaining >10-fold higher than the IC90 for virus neutralization for at least 8 days (Figure S11A). Half-lives of the proteins were extended ($t_{1/2\beta}$ = 124 and 224 h for sACE2$_2$.v2.4-IgG1(YTE) and sACE2$_2$.S19-IgG1(YTE), respectively) and exposures were increased by an order of magnitude (AUC_{0-192h} = 4100 and 6400 μg/mL × h, respectively) (Table 2). Decoy receptors produced from stable CHO expression are thus expected to have highly favorable properties *in vivo* for efficacy.

In the aforementioned study, the PK profiles were insufficiently characterized for modeling PK profiles in humans. We therefore

Table 3. Sialylation of decoy receptors purified from different sources

$sACE2_2$-IgG1 protein[a]	Source	Neu5Ac[b]	Neu5Gc[c]
$sACE2_2$.v2.4-IgG1(YTE)	Expi293F	8.3	Not detected
$sACE2_2$.S19-IgG1(YTE)	Expi293F	7.1	Not detected
$sACE2_2$.v2.4-IgG1(YTE)	CHOK1SV GS-KO	14.4	0.46
$sACE2_2$.S19-IgG1(YTE)	CHOK1SV GS-KO	14.8	0.50

[a]Measured by RP-HPLC.
[b]Mol Neu5Ac/mol protein monomer. Limit of detection is 2.2 mol/mol protein.
[c]Mol Neu5Gc/mol protein monomer. Limit of detection is 0.12 mol/mol protein.

repeated PK assessment of $sACE2_2$.S19-IgG1(YTE) from CHOK1SV GS-KO stable pools under the same conditions but with plasma exposures measured out to 14 days (Figure S11B). A second group of mice was administered the same dose of $sACE2_2$.S19-IgG1(YTE) subcutaneously in the flank. Plasma concentrations of $sACE2_2$.S19-IgG1(YTE) following i.v. or s.c. administration converged at later time points and bioavailability via s.c. route was high (72%). PK parameters following i.v. administration were lower in this experiment ($t_{1/2\beta}$ = 122 and AUC_{0-336h} = 8540 μg/mL × h; Table 2) either due to experimental variability or better characterization of PK parameters from inclusion of longer time points. Compartmental PK parameters after i.v. dosing were calculated and used to predict human PK parameters using the fixed exponent approach (Table S13). Human PK modeling predicts that 7.3 mg/kg and 22 mg/kg i.v. doses will maintain plasma concentrations of $sACE2_2$.S19-IgG1(YTE) above the IC90 and 3 × IC90 for 12 weeks, respectively (Figure S11C). These are feasible doses similar to those of prophylactic antibodies and suggests dosing intervals close to 3 months are achievable for long-term prophylaxis or a single dose may provide protection over a season.

The optimized decoys have low probability of presenting immunogenic epitopes on HLA class II

The engineered decoy receptors differ by a small number of mutations from wild-type ACE2 and hence might be immunogenic. It is noteworthy that soluble decoy receptors for other indications are safe and widely prescribed,[66] and at least wild-type sACE2 without any fusion partner is nonimmunogenic and well tolerated in human patients.[67–70] While immunogenicity in human patients is hard to predict, it would be concerning if the decoys are processed to present neoepitopes on Human Leukocyte Antigen class II (HLA-II) that stimulate CD4+ T cells.[71,72] Activated CD4+ T cells promote B cell activation, proliferation, and antibody affinity maturation and class switching. Using an algorithm trained on large empirical datasets,[73] the sequences of $sACE2_2$-IgG1 decoys were scanned for peptides predicted to be displayed on a set of 14 common HLA-II allotypes. Here, peptides that fall within the top 10% of all possible sequences for calculated binding affinity and are predicted to bind a minimum threshold of four HLA-II allotypes are considered to have a high probability of being presented on HLA-II. Compared with wild-type $sACE2_2$-IgG1, engineered $sACE2_2$.v2.4-IgG1 has three mutations: there are no high-affinity antigenic peptides predicted to encompass the ACE2-T27Y mutation, the ACE2-L79T mutation may be found at the end positions of a small number of presented peptides, and ACE2-N330Y is predicted to remove an HLA-II epitope (Figure 5A). In $sACE2_2$.S19-IgG1, there are three more mutations in addition to the v2.4 set: ACE2-V491I falls within a predicted epitope but is a highly conservative change of a single methyl group, while the mutations that add N-glycans at residues 660 and 718 were not analyzed as the computational algorithm is not trained on glycopeptides. The YTE mutations in the Fc region remove a predicted HLA-II epitope (Figure 5A) and are known to be safe in antibodies approved for clinical use.

To experimentally validate the *in silico* analysis, we expressed 17-mer peptides from ACE2 centered on each mutated position by yeast surface display and analyzed their binding to a panel of common HLA-DP, HLA-DQ, and HLA-DR alleles.[74–76] For example, to analyze the effect of mutation T27Y, we expressed peptides corresponding to ACE2 residues 19 to 35 with the wild-type amino acid (Thr27) or mutated amino acid (Tyr27) at the central position. By choosing 17-mer long peptides, all possible core 9-mers[77] that might bind HLA-II are covered where the central residue occupies any of positions P1 to P9. Soluble HLA-II proteins were prepared bound to the CLIP placeholder peptide (or an equivalent peptide)[78] and were incubated with yeast displaying wild-type and mutant ACE2 peptides. Under acidic conditions in the presence of the class II-specific chaperone HLA-DM, the CLIP placeholder peptide was exchanged for the yeast-displayed ACE2 peptide in a loading reaction that recapitulates the biochemistry of the antigen presentation pathway.[79] Bound HLA-II was then detected by fluorescent antibody staining and flow cytometry. High levels of bound HLA-II are detected in positive control peptides matched to specific HLA-II alleles and polyserine functions as a negative control peptide (Table S14). Data from the assay are highly reproducible (Figure 5B).

Based on the peptide-HLA-II binding assay and in agreement with *in silico* analysis, the three ACE2 mutations in $sACE2_2$.v2.4-IgG1 are considered low risk (Figure 5C). The ACE2 peptide centered at position 27 is not bound by any of the common HLA-II alleles in the test set; the peptide centered at position 79 is weakly bound by HLA-DRB4 but the interaction is diminished by the L79T mutation; and only the peptide centered at position 330 displays tight HLA-II binding, although again to just a small number of alleles (HLA-DPB2 and HLA-DPB4) and the N330Y mutation weakens the interaction. Similarly, conservative mutation V491I in $sACE2_2$.S19-IgG1 is located in a region of ACE2 that is poorly bound by HLA-II. The two mutations in $sACE2_2$.S19-IgG1 that introduce glycosylation sites, M662T and N720S, are located in regions that weakly to moderately bind multiple HLA-II alleles and thus might be considered higher immunogenicity risks. However, binding of the M662T and N720S vs. wild-type peptides is substantially decreased across the whole set of HLA-II alleles, suggesting the neo-glycopeptides of $sACE2_2$.S19-IgG1 are poorly presented. Overall, the mutations introduced into ACE2 are not anticipated to be strongly immunogenic.

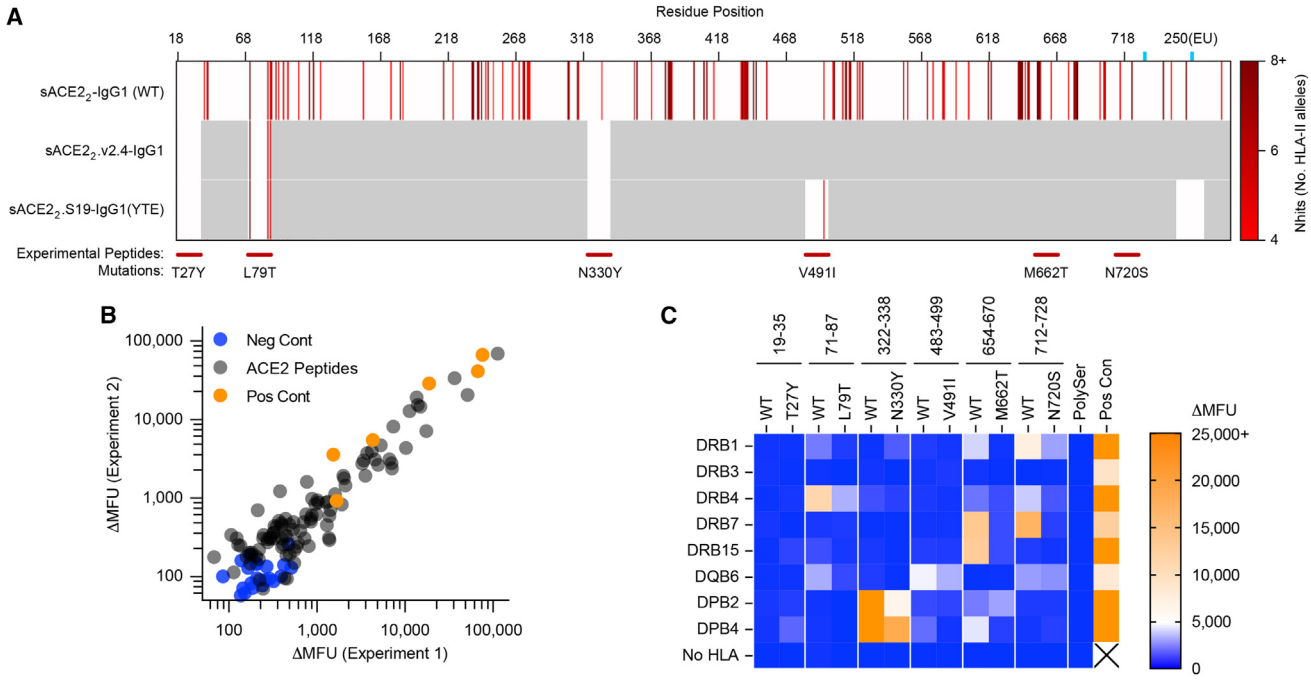

Figure 5. The v2.4 and S19 mutations in ACE2 are predicted to have low immunogenicity

(A) Computational analysis of calculated affinity of peptides to HLA-II allotypes. The wild-type sACE2$_2$-IgG1 sequence (top row) is scanned for peptides predicted to be displayed on a common set of 14 HLA-II allotypes. In this analysis, the minimum threshold for a peptide to be considered an antigen is predicted affinity for four HLA-II allotypes (Nhits ≥4) from a set of 14 common alleles. For sACE2$_2$-IgG1 derivatives, the sequence is grayed out except for the regions where mutations are introduced to highlight whether a mutation is within a predicted epitope and/or changes the probability of presentation. Peptides that were analyzed experimentally by yeast display are indicated below with dark red bars. (B) Peptides were displayed on yeast and binding to HLA-II following an HLA-DM-dependent peptide loading reaction was measured by flow cytometry. The correlation plot shows the agreement between two independent replicates measuring mean fluorescence units (MFU) for bound HLA-II. Polyserine negative control reactions are blue, positive control peptide/HLA-II pairs are orange, and ACE2 peptides are gray. (C) Yeast display measurements of HLA-II binding to ACE2 peptides is plotted from no signal (dark blue) to high binding signal (orange).

The optimized decoys broadly bind to S proteins of omicron sublineages

Numerous variants of the SARS-CoV-2 omicron lineage have evolved, with mutations arising in the S gene that influence ACE2 binding and immune evasion. We previously demonstrated that sACE2$_2$-IgG1 carrying the v2.4 mutations binds with high affinity and neutralizes BA.1, BA.2, and BA.4/BA.5 omicron sublineages and protects human ACE2 transgenic mice from death and weight loss following infection with a high dose of BA.1 omicron SARS-CoV-2.[27] Others have independently shown that the v2.4 mutations enhance sACE2 affinity for S protein and *in vitro* neutralization potency against BQ.1.1 and XBB omicron sublineages.[80] Here, we confirm that the optimized decoy receptors remain highly active for tight binding to S proteins of omicron sublineages. Binding of decoy receptors to S protein is tightly correlated with neutralization activity.[15,25,27,80] Using flow cytometry to measure avid binding of decoy receptors to trimeric S proteins expressed at the plasma membrane, sACE2$_2$.v2.4-IgG1(YTE) and sACE2$_2$.S19-IgG1(YTE) were shown to tightly bind the S proteins of BF.7, XBB, BA.2.75.2, and BQ.1.1 omicron sublineages at low nanomolar concentrations (Figure S12A). Binding of the optimized decoy receptors across the panel of S proteins was almost an order of magnitude tighter than that of wild-type sACE2$_2$-IgG1 in this assay. Furthermore, sACE2$_2$.v2.4-IgG1(YTE) and sACE2$_2$.S19-IgG1(YTE) were equally potent at neutralizing XBB.1.5 pseudovirus (Figure S12B). Exceptional breadth of the decoy receptors is thus maintained following modifications for improved pharmacokinetics.

DISCUSSION

Decoy receptors for SARS-CoV-2 have been engineered for tight affinity to Spike and potent virus neutralization, yet beyond fusion with the immunoglobulin Fc region for half-life extension, the properties governing their pharmacokinetics have not been explored. We show here that long half-life and high exposure of the sACE2$_2$.v2.4-IgG1 decoy receptor are dependent on sialylation of glycans. The expected efficacy of a decoy receptor in treating or preventing SARS-CoV-2 infection will thus strictly depend on how the protein is manufactured. We demonstrate that high sialylation of decoy receptors is accomplished when expressed by CHOK1SV GS-KO stable cells, an expression system that has been used for the production of approved biologic drugs, without any loss in S affinity. Furthermore, the sequence of the decoy receptor was optimized by inclusion of mutations in the Fc region that reduce dissociation from FcRn and by the addition of custom N-glycosylation sites to the ACE2 CLD. The final

half-life of the optimized decoy receptor following i.v. administration in humanized FcRn mice was 5–9 days and exposures were increased by orders of magnitude over the poorly sialylated starting material.

The terminal monosaccharides of complex glycans on glycoproteins are often sialic acid, which masks underlying galactose residues that are recognized by asialoglycoprotein receptors that are highly expressed in the liver.[81,82] In seminal research 50 years ago, hydrolytic removal of sialic acids from serum glycoproteins was shown to lead to their rapid clearance from circulation within minutes.[83] Sialylation can also be important for regulating the half-lives of therapeutic glycoproteins.[81,82] Of special note, etanercept (approved for several autoimmunity indications) is a decoy receptor formed by the fusion of the soluble TNFR2 ectodomain to the Fc of IgG1 and thus closely resembles sACE2-IgG1 decoys. Serum levels of poorly sialylated forms of etanercept are decreased by three orders of magnitude following s.c. or i.v. administration in rats,[84] mimicking our observations of sACE2-IgG1 decoys. While many studies have investigated mutations of sACE2-IgG1 decoys to increase their neutralization potency, we now demonstrate that *in vivo* properties depend on more than the protein's amino acid sequence and are also heavily impacted by how the protein is expressed and glycosylated. Indeed, the glycosylation properties of the decoy receptors (specifically the presence of sialic acid sugars) had far greater impact on the proteins' PK than any of the amino acid substitutions that were made to the ACE2 or IgG1 Fc moieties, including substitutions to introduce glycosylation sites in ACE2 and the YTE mutations in IgG1 Fc. In the large amount of literature published describing and characterizing ACE2 decoy receptors for COVID-19, we are not aware of any reports where sialylation or the cell line for protein production were considered for PK optimization. Rather, multiple studies have reported glyco-engineered ACE2 decoy receptors in which glycans and sialic acids were modified or removed to enhance *in vitro* neutralization activity,[85–87] while our findings would suggest such modifications are devastating to *in vivo* pharmacokinetic properties.

Based on *in silico* and biochemical analyses of peptide epitope binding to HLA-II, we conclude that $sACE2_2$.v2.4-IgG1 and $sACE2_2$.S19-IgG1 have low immunogenicity risk. However, these assessments examine a single aspect of the immunological events that lead to generation of anti-drug antibodies. Immunogenicity of protein drugs is also affected by proteolytic processing within antigen-presenting cells, the prevalence of naive T cell and B cell receptors that engage antigenic epitopes, tolerance, allele-specific HLA-II peptide repertoire selection, product formulation and aggregation, dose, and route of administration.[88] COVID-19 patients also have high levels of circulating, low-activity sACE2 due to endogenous receptor shedding during SARS-CoV-2 infection and promiscuous anti-ACE2 autoantibodies are common,[47,51,89] as are autoantibodies to other immune modulators and factors in severe COVID-19.[89–93] Due to these complexities, the possible immunogenicity of engineered ACE2 decoy receptors will remain an open question until human clinical data are available. Promisingly, recombinant wild-type sACE2 has never been found to be immunogenic across multiple clinical trials.[67–70]

Recombinant human sACE2 was developed as an investigational drug for acute respiratory distress syndrome (ARDS)[67,68] and had partial efficacy on secondary endpoints in a phase 2 trial of hospitalized patients with severe COVID-19 requiring invasive mechanical ventilation (ClinicalTrials.gov Identifier NCT04335136).[22] The protein used in this trial was a wild-type ACE2 with comparatively low S affinity and a short half-life compared with engineered decoys like $sACE2_2$.v2.4-IgG1 and $sACE2_2$.S19-IgG1. At the doses administered to patients, drug concentrations in serum never reached above the IC90 for virus neutralization[94,95] for any appreciable period of time,[68] and we speculate that what benefits were observed in patients were due to ACE2 catalytic activity rather than virus neutralization. We have shown both here and previously[27] that ACE2 decoy receptors in which catalytic activity is completely knocked out partially lose therapeutic efficacy in the K18-hACE2 mouse model of COVID-19. This may indicate that ACE2 catalytic activity contributes to optimal protection of mice from lethal SARS-CoV-2 infection, although we note that the catalytic dead ACE2 decoy receptor also suffers from reduced plasma half-life and exposure. It is noteworthy that a key product of ACE2 catalysis, Ang(1–7), is markedly reduced in the plasma of COVID-19 patients, as is the catalytic activity of sACE2 present in saliva and plasma.[50,51] Decreased ACE2 activity, as inferred by reduced Ang(1–7) in plasma, is closely correlated with COVID-19 severity (hospitalization and oxygen supplementation), as well as elevated inflammatory cytokines and d-dimer, a biomarker of coagulopathy.[50] If catalytic activity of ACE2 decoy receptors does contribute to therapeutic efficacy, it would provide a unique mechanism of action that differentiates this class of drug candidates from monoclonal antibodies.

Others have argued that catalytically active ACE2 decoy receptors pose an unacceptable safety risk and are developing inactive ACE2 variants that function solely to neutralize infection (reviewed in Jing and Procko[19]). Recombinant wild-type sACE2 was well tolerated by human subjects in six clinical trials (ClinicalTrials.gov Identifiers NCT04335136, NCT00886353, NCT05065645, NCT03000686, NCT01597635, NCT03177603) and we are unaware of reports describing acute ACE2-related toxicity in animal studies at therapeutically relevant doses. Notably, blood pressure is unaffected in human subjects receiving recombinant sACE2, despite on-target cleavage of angiotensin II to Ang(1–7),[69] which challenges the assumption that treatment with active ACE2 decoy receptors will cause dangerous hypotension. Inhibitors of ACE, an enzyme that is upstream of ACE2 in the renin-angiotensin-aldosterone system and is therefore expected to have broader biological effects, are prescribed to >10 million people in the United States.[96] While hypotension occurs in one in 33 patients taking ACE inhibitors,[97] it is an uncommon cause of drug discontinuation.[98,99] In summary, the hypothetical safety risks associated with ACE2 catalytic activity are not supported by preclinical or clinical evidence and are likely to be infrequent.

Overall, we identify a critical molecular attribute (sialylation) of sACE2 decoy receptors that must be considered in their production to maximize *in vivo* efficacy and also show how other modifications,

including the addition of custom glycosylation sites, can improve pharmacokinetics. These findings are likely important for the development of other decoy receptors that are heavily glycosylated.

MATERIALS AND METHODS

Rosetta-based stability design

Stability was optimized using an *in silico* rational protein engineering approach based on the cryo-EM structure of human ACE2 (PDB: 6M17). Stabilizing mutations in ACE2 were identified using the Rosetta software package.[52] First, truncated models of ACE2 monomers (amino acids [a.a.] 21–615 and 21–732) underwent backbone and sidechain optimization via Rosetta Relax with score function ref. 2015. The protocol performed site saturation mutagenesis for both relaxed construct models, allowing neighboring amino acids to repack around a mutated residue as described previously.[100] The mutants were ranked according to the difference in score between the wild-type amino acid and the substitutions. Mutations with residues near the ACE2 active site, at the interface with SARS-CoV-2 RBD, or conserved between human and mouse ACE2 were excluded, thus focusing design to residues that were expected to tolerate substitutions. Visual/manual inspection was performed for final selection of protein variants.

N-glycosylation site design

N-glycosylation sites require a specific motif: Asn-X-Ser/Thr, where X is any amino acid other than proline. The previously described Rosetta-generated mutational data allowed for the identification of energetically favorable substitutions that result in an N-glycosylation motif. Potential glycosylation sites were selected based on (1) Rosetta score, (2) minimal number of mutations compared with original sequence, (3) preference for Thr compared with Ser at the third position due to enhanced glycosylation efficiency, and (4) comparison to the mouse ACE2 sequence (UniProtKB - Q8R0I0), which suggested glycosylation sites unlikely to disrupt folding/function.

Disulfide design

Disulfide bonds require specific geometric constraints for formation. The disulfidizer mover within Rosetta substitutes all pairs of residues with Cys to evaluate proper geometries for disulfide formation.[101] Those that satisfied this geometric constraint were then sorted by disulfide score (dslf_fa13) and visually inspected.

Immunogenicity prediction

Immunogenicity assessment is based on *in silico* prediction of HLA-II presentation of peptides from $sACE2_2$-IgG1 variants using a tool trained on experimental peptide-HLA-II datasets.[73] The 14 HLA-II allotypes that were used in this analysis are HLA-DRB1*01:01, HLA-DRB1*03:01, HLA-DRB1*04:01, HLA-DRB1*07:01, HLA-DRB1*08:02, HLA-DRB1*11:01, HLA-DRB1*13:02, HLA-DRB1*15:01, HLA-DRB1*09:01, HLA-DRB3*01:01, HLA-DRB4*01:01, HLA-DRB5*01:01, HLA-DQA1*05:01-DQB1*03:01, and HLA-DQA1*03:01-DQB1*03:02. Peptides that fell within the top 10% of all possible sequences for calculated binding affinity and were predicted to bind a minimum threshold of four HLA-II allotypes were identified as potentially immunogenic.

Cell lines and transfection

Expi293F cells (Thermo Fisher) were cultured at 37°C, 125 rpm, 8% CO_2, in Expi293 Expression Medium (Thermo Fisher). Expi293F were transfected at a density of 2×10^6 mL^{-1} with 0.5–1.0 μg plasmid DNA per mL of culture using ExpiFectamine (Thermo Fisher) according to the manufacturer's directions. ExpiFectamine Transfection Enhancers 1 (5 μL per mL of culture) and 2 (50 μL per mL of culture) were added ∼18 h post-transfection and medium was collected on day 5–7. ExpiCHO-S cells (Thermo Fisher) were cultured at 37°C, 125 rpm, 8% CO_2, in ExpiCHO Expression Medium (Thermo Fisher). ExpiCHO-S were transfected at a density of 6×10^6 mL^{-1} with 1.0 μg plasmid DNA per mL of culture using ExpiFectamine CHO Reagent (Thermo Fisher) according to the manufacturer's directions. ExpiFectamine CHO Enhancer (6 μL per mL of culture) and ExpiCHO Feed (240 μL per mL of culture) were added ∼20 h later and the temperature was lowered (33°C). ExpiCHO Feed (240 μL per mL of culture) was added again on day 5. CO_2 was decreased stepwise on days 9–12 to 5% final. The medium was harvested on days 12–14.

Plasmids

The expression plasmid for $sACE2_2$.v2.4-IgG1 is previously described[25] and deposited with Addgene (# 154106). Briefly, the coding sequence is ligated into the NheI-XhoI sites of pcDNA3.1(+) (Invitrogen) and encompasses human ACE2 (GenBank: NM_021804.1) amino acids (a.a.) M1-G732 fused via a 1×serine linker to human IgG1 Fc a.a. D221-K447 (nG1m1 isoallotype; GenBank: KY432415.1). Targeted mutations were introduced by overlap extension PCR and confirmed by Sanger sequencing.

Spike (S) sequences were subcloned from plasmid pCEP4-myc-S (Wuhan variant; Addgene # 169846) using overlap extension PCR to introduce mutations. The assembled PCR products were cloned into the NheI-XhoI sites of pcDNA3.1(+). The final plasmids encode the mature S proteins (a.a. V16-T1273; numbering based on Wuhan variant S protein in GenBank: YP_009724390.1) downstream of an influenza HA signal peptide and N-terminal myc epitope tag. The mutations in the S proteins of SARS-CoV-2 variants used in this study are as follows. Omicron sublineage BA.2.75.2: T19I, Δ24–26, A27S, G142D, K147E, W152R, F157L, I210V, V213G, G257S, G339H, R346T, S371F, S373P, S375F, T376A, D405N, R408S, K417N, N440K, G446S, N460K, S477N, T478K, E484A, F486S, Q498R, N501Y, Y505H, D614G, H655Y, N679K, P681H, N764K, D796Y, Q954H, N969K, and D1199N. Omicron sublineage XBB: T19I, A27S, V83A, G142D, H146Q, Q183E, V213E, G252V, G339H, R346T, L368I, S371F, S373P, S375F, T376A, D405N, R408S, K417N, N440K, V445P, G446S, N460K, S477N, T478K, E484A, F486S, F490S, Q498R, N501Y, Y505H, D614G, H655Y, N679K, P681H, N764K, D796Y, Q954H, and N969K. Omicron sublineage BF.7: T19I, Δ24–26, A27S, Δ69-70, G142D, V213G, G339D, R346T, S371F, S373P, S375F, T376A, D405N, R408S, K417N,

N440K, L452R, S477N, T478K, E484A, F486V, Q498R, N501Y, Y505H, D614G, H655Y, N679K, P681H, N764K, D796Y, Q954H, and N969K. Omicron sublineage BQ.1.1: T19I, Δ24–26, A27S, Δ69-70, G142D, V213G, G339D, R346T, S371F, S373P, S375F, T376A, D405N, R408S, K417N, N440K, K444T, L452R, N460K, S477N, T478K, E484A, F486V, Q498R, N501Y, Y505H, D614G, H655Y, N679K, P681H, N764K, D796Y, Q954H, and N969K.

Protein purification

Expression medium was centrifuged (800 × *g*, 4°C, 10 min) to remove cells and the pH adjusted to 7.5 with 1M Tris base. Insoluble particulates were removed by centrifugation (15,000 × *g*, 4°C, 20 min). The supernatant was incubated with KanCapA resin (Kaneka Corporation; 2 mL resin per 100 mL medium) for 1–2 h at 4°C. Resin was collected by passing through a chromatography column and washed with 10 column volumes (CV) of Dulbecco's phosphate-buffered saline (PBS). Fc-fusion proteins were eluted with 4 CV 60 mM sodium acetate pH 3.7 and rapidly neutralized by collecting in 2 CV 1M Tris pH 8.0. The pH was further raised to ∼7.5 with an additional 1–2 CV 1M Tris base. Eluted proteins were concentrated with a centrifugal filtration device and injected on a Superdex 200 gel filtration column (Cytiva) equilibrated with PBS. Peak fractions were pooled, concentrated, and protein aliquots snap frozen in liquid nitrogen for storage at −80°C. Concentrations were determined using calculated extinction coefficients and absorbance at λ = 280 nm.

Pharmacokinetics in human FcRn mice

Male B6.Cg-Fcgrt^{tm1Dcr} Tg(FCGRT)32Dcr/DcrJ mice (JAX stock # 014565; 6–8 weeks old; three mice per group) were housed in ventilated cages with HEPA filtered air and provided filtered tap water (pH 2.5–3.0) and standard lab chow ad libitum. Artificial fluorescent lighting was on a 12 h light/dark cycle, temperature 20°C–26°C and humidity 30%–70%. Animals were administered proteins diluted in PBS and sterile filtered for a final injection volume of 4 mL/kg via i.v. (tail vein) or s.c. (flank). In life blood was collected via a retroorbital route into heparin tubes. At terminal time points, mice were euthanized via CO_2 asphyxiation and blood was collected via cardiocentesis into heparin. Processed plasma samples were stored at −80°C until analysis for ACE2 catalytic activity or decoy receptor concentration by ELISA. Experiments were conducted under institutional review and IACUC approval at JAX or at Bloodworks Northwest Research Institute. Pharmacokinetic parameters were fitted with PKSolver 2.0 using the linear trapezoidal method.

Compartmental modeling of human FcRn mouse PK data

Since the PK samples were obtained using a staggered sampling scheme, the mean composite data for each dose group were used for modeling. The Tg32 mouse data were best fit with an i.v. bolus 2-compartment model with $1/\hat{y}^2$ weighting. The resulting compartmental PK parameters for each dose group are shown in Table S13. Human PK parameters were predicted from Tg32 mouse PK data using the fixed exponent approach ($CL_{human} = CL_{animal} \times [BW_{human}/BW_{animal}]^y$ and $V_{human} = V_{animal} \times [BW_{human}/BW_{animal}]^z$; method from Wang and Prueksaritanont[102]). PK parameters were scaled with an exponent of 0.9 for CL and 1.0 for V.[103] The predicted human PK parameters are shown in Table S13 and were used to predict human PK profiles at different doses.

ACE2 catalytic activity assay

Hydrolysis of a quenched fluorescent peptide substrate was measured on a Biotek Cytation 5 plate reader with the Fluorometric ACE2 Activity Assay Kit (BioVision) according to the manufacturer's directions.

Biolayer interferometry

For measuring kinetics of $sACE2_2$-IgG1/RBD interactions, responses were recorded on an Octet RED96a and analyzed with a 1:1 binding model (global fit) using instrument software (Sartorius). $sACE2_2$-IgG1 proteins were immobilized at 100 nM for 60 s to AHC (anti-human IgG Fc) biosensors (Sartorius) in assay buffer (10 mM HEPES pH 7.6, 150 mM NaCl, 3 mM EDTA, 0.05% polysorbate 20, 0.5% non-fat dry milk). Loaded sensors were equilibrated in assay buffer, transferred to RBD-8h solutions to measure association, and transferred back to buffer to measure dissociation. The purification of RBD proteins is previously described.[15]

For measuring kinetics of $sACE2_2$-IgG1/FcRn interactions, responses were recorded on a Gator Bio Prime and analyzed with a 1:1 binding model (global fit) using instrument software (Gator Bio). FcRn with a C-terminal 6×His-tag and complexed with beta-2-microglobulin (R&D Systems) was immobilized on anti-his biosensors (Gator Bio) to reach a response of 1 nm. The biosensors were equilibrated for 120 s to achieve a stable baseline in PBS containing 0.1% Tween 20 plus 0.2% bovine serum albumin at pH 6.0 or pH 7.4. Biosensors were then transferred to $sACE2_2$-IgG1 solutions in the same buffer for association kinetics and back to buffer for dissociation kinetics.

Sandwich ELISA

Nunc MaxiSorp plates (Invitrogen) were coated overnight with donkey anti-human Fcγ (Jackson, Cat. No. 709-005-098) at 0.3 μg/mL in PBS. The plates were washed 4× with PBS containing 0.05% Tween 20 (PBS-T). Purified protein standards were prepared in mouse plasma. Samples and standards were diluted in PBS and incubated in wells for 1 h at room temperature. Plates were washed 4× with PBS-T and wells were incubated for 1 h at room temperature with 0.3–1.0 μg/mL polyclonal goat anti-human/mouse/rat/hamster ACE2 antibody (R&D Systems, Cat. No. AF933-SP) in PBS. Plates were washed 4× with PBS-T and incubated 1 h at room temperature with 1:25,000 donkey anti-goat (H + L) antibody-HRP conjugate (Fisher, cat. no. PA128664) in PBS. Plates were washed 4× with PBS-T and developed with One Step TMB Ultra (Thermo Fisher) for 20 min. The reaction was ended with ELISA Stop Solution (Thermo Fisher) and absorbance at λ = 450 nm read on a Biotek Cytation 5.

Glycomics and glycopeptidomics

Analysis methods were previously described.[53] They are briefly outlined here.

For glycomics analysis, glycoproteins were diluted with 50 mM ammonium bicarbonate buffer, reduced with DTT, alkylated with iodoacetamide, and desalted with 10 kDa molecular weight cutoff centrifugal filtration devices. N-Glycans were released with PNGaseF (37°C for 48 h) and permethylated. After the removal of N-glycans, the O-glycans were removed by beta elimination and samples were treated with 50 mM sodium hydroxide and sodium borohydride for 18 h at 45°C. The released O-glycans were purified by Dowex H+ form ion exchange resin, lyophilized, borates were removed by a stream of nitrogen gas, and O-glycans were permethylated. Permethylated N- and O-glycans were analyzed by MALDI-TOF-MS. N- and O-glycan structures were assigned using Glycoworkbench software based on precursor masses (sodiated) and the common mammalian biosynthetic pathway.

Glycopeptide analysis and site mapping were performed using liquid chromatography tandem mass spectrometry. Glycoprotein samples were reduced with DTT, alkylated with iodoacetamide, and digested with 0.5 μg/μL sequencing-grade trypsin at 37°C for 16 h. Peptides were analyzed on an Ultimate 3000 RSLCnano connected to a Thermo Eclipse mass spectrometer. Nano-LC columns of 15-cm length with 75-μm internal diameter, filled with 3 μm C18 reverse-phase material were used for chromatographic separation of the samples. The separation conditions were low to high acetonitrile in a solution containing 0.1% formic acid, and the separation time was 1 h. The precursor ion scan was acquired at 120,000 resolution in the Orbitrap analyzer and precursors at a time frame of 3 s were selected for subsequent fragmentation using HCD. Charge state screening was enabled, and precursors with unknown charge state or a charge state of +1 were excluded. Dynamic exclusion was enabled (exclusion duration of 30 s). The fragment ions were analyzed on an Orbitrap for HCD at 30,000 resolution. The glycoproteomic data were processed with Byonic (v4.0.12) and searched against the sequences and a catalog of more than 180 N-glycans and nine common O-glycans. The precursor mass tolerance and fragment mass tolerances were set to 5 ppm and 10 ppm, respectively. Additional modifications including deamidation of N and Q, carboxymethylation of C, and oxidation of precursor were also included in the search. Assignments were made using Byonic software (Delta Mod. Score $\geq$10, Log Prob>3) and manual interpretation. Raw files retrieved from nanoLC-MS were deconvoluted in Xcalibur 4.1. Monoisotopic peak areas for each glycopeptide found in Byonic were manually pooled in FreeStyle 1.8. The relative percentages of each glycoform were determined by deconvolution of the liquid chromatography-mass spectrometry data at the full MS level, then determining the area under the curve for each full MH+. Relative abundance was calculated in Excel. Suggested glycan structures were predicted in Glycoworkbench and GlyConnect. Glycoforms are based on the assumed biosynthetic pathway.

Deglycosylation

Purified $sACE2_2$.S19-IgG1(YTE) from Expi293F culture was deglycosylated in PBS under native conditions for 20 h at room temperature. For PNGase F treatment, substrate protein (5 mg/mL) was incubated with PNGase F (New England Biolabs; 125 units/μL) in 1× Glycobuffer (New England Biolabs) prepared in PBS. For neuraminidase treatment, substrate protein (6.8 mg/mL) was incubated with *Arthrobacter ureafaciens* neuraminidase (Roche; 1.7 units/mL) in PBS. Mixtures were separated on a Superdex 200 gel filtration column to purify the treated $sACE2_2$.S19-IgG1(YTE) proteins.

Differential scanning fluorimetry

Purified proteins were analyzed for thermostability via DSF using the Protein Thermal Shift dye kit (Thermo Fisher) on an Applied Biosystems QuantStudio3 (Thermo Fisher) according to manufacturer's instructions with a final protein concentration of 0.21 mg/mL. Melting temperature was determined using Thermal Shift software and Boltzmann Tm is reported from quadruplicate measurements.

Flow cytometry assay for Spike binding

Expi293F cells were transfected with 500 ng pcDNA3-myc-S plasmid per ml of culture using ExpiFectamine as described above. Cells were harvested (600 × *g*, 1 min) 24 h post-transfection without the addition of transfection enhancers. Cells were washed with cold PBS supplemented with 0.2% bovine serum albumin (PBS-BSA) to reduce non-specific binding. Cells were resuspended in PBS-BSA and incubated with serial dilutions of $sACE2_2$-IgG1 proteins on ice for 30 min. Cells were washed with PBS-BSA and were resuspended in 1:150 polyclonal chicken anti-MYC-FITC (Immunology Consultants Laboratory) and 1:300 anti-human IgG-APC (clone HP6017, BioLegend) for 30 min on ice. Cells were washed twice with PBS-BSA and analyzed on a BD Accuri C6 flow cytometer. The main population of viable cells was gated by forward and side scatter. Mean APC fluorescence was recorded for the myc-positive population. Background fluorescence of transfected cells incubated without $sACE2_2$-IgG1 proteins was subtracted and data were normalized based on the total fluorescence signal for each experiment.

BSL-3 study approval and SARS-CoV-2 viruses

All aspects of working with live SARS-CoV-2 in animals were approved by the office of Environmental Health and Safety, Institutional Animal Care and Use Committee, and Regional Biocontainment Laboratory (RBL) at University of Pittsburgh prior to study initiation. SARS-CoV-2 experiments were performed at biosafety level 3 (BSL-3) conditions at RBL in the Center for Vaccine Research at the University of Pittsburgh by personnel equipped with powered air-purifying respirators. CDC/2019n-CoV/USA_WA1/2020 virus was propagated in Vero E6 cells (CRL-1586, American Type Culture Collection, ATCC). The supernatant was collected upon observation of cytopathic effect. Debris was removed by centrifugation. Supernatant was then aliquoted and stored at −80°C. Virus titers were quantitated by a plaque-forming assay using Vero E6 cells.

Inoculation of SARS-CoV-2 in K18-hACE2 transgenic mice

Hemizygous K18-hACE mice with c57BL/6J background (strain #034860: B6.Cg-Tg(K18-ACE2)2Prlmn/J) were purchased from The Jackson Laboratory. Animals were housed in groups and fed standard chow. Mice (8–10) weeks old inhaled with isoflurane were

inoculated intranasally with 1×10^4 PFU (plaque-forming units) of SARS-CoV-2 isolate WA1 in sterile PBS for 50 μL per mouse. Twenty-four hours post-inoculation, $sACE2_2$.S19-IgG1(YTE), $sACE2_2$.S19 RD-IgG1(YTE), or IgG1 control was administered at 10 mg/kg via retroorbital injection. The IgG1 is an isotype-matched control antibody (InVivoPlus human IgG1 isotype control, Cat. No. BP0297, Bio X Cell).

Lung harvest and mRNA expression by quantitative real-time PCR

Mice were anesthetized with ketamine/xylazine (100/10 mg/kg) and mouse lungs were harvested after 10 mL PBS perfusion at day 7 post-inoculation. RNA was extracted from homogenized lung tissues using TRIzol Reagent (Thermo Fisher) according to the manufacturer's protocol. RNA was quantified by Nanodrop 1000 (Thermo Fisher) and reverse transcribed into cDNA using High-Capacity cDNA Reverse Transcription Kit (Thermo Fisher). FastStart Universal SYBR Green Master Mix (Thermo Fisher) and gene-specific primers (Table S15) were used to detect expression levels of SARS-CoV-2 Spike, Nsp, and PPIA on the Bio-Rad Real-Time PCR System (Bio-Rad). The relative transcript levels of SARS-CoV-2 Spike or Nsp are calculated by $2^{-\Delta Ct}$, where ΔCT is calculated by subtracting the cycle threshold (CT) value of the gene of interest from the CT of the housekeeping gene PPIA.

Stable pooled expression in CHOK1SV GS-KO cells

Genes encoding $sACE2_2$.v2.4-IgG1(YTE) and $sACE2_2$.S19-IgG1(YTE) were designed with a consensus Kozak sequence and codon optimized for *Cricetulus griseus*. Genes were synthesized by Geneart AG and subcloned into the HindIII and EcoRI sites of pPV-A (Lonza Biologics). The pPV-A part vectors were assembled into piggyBac destination vectors (Lonza Biologics) in an assembly reaction containing a 2:1 ratio of part vector to destination vector, T4 DNA ligase, and Esp3I. The reaction was cycled between 37ºC and 16°C for the digestion and ligation phases of the assembly reaction, respectively.

CHOK1SV GS-KO cells (Lonza Biologics) were cultured in CD-CHO media (Life Technologies) supplemented with 6 mM L-glutamine. Cells were grown at 36.5°C, 5% CO_2, 85% humidity, 140 rpm. Cells were transfected via electroporation using the Bio-Rad Gene Pulse XCell; 1×10^7 cells in 700 μL CD-CHO medium were combined with 100 μL (40 μg) linearized DNA and 5 μg piggyBac Transposase mRNA (Lonza Biologics) in a 0.4-cm gap electroporation cuvette and pulsed at 300 V, 900 μF. Cells were transferred to 30 mL pre-warmed CD-CHO supplemented with 1% SP4 (Lonza Biologics) to generate a stable pool and incubated at 36.5°C, 5% CO2, 85% humidity, 140 rpm. Three stable pool transfectants were established per gene, one of which was a no-mRNA control. Once the density was $>1 \times 10^6$ cells/mL, stable recombinant CHOK1SV GS-KO cells were maintained in CD-CHO media supplemented with 50 μM L-methionine sulfoximine (Sigma-Aldrich) and 1% SP4 (Lonza Biologics).

Clarified and 0.22-μm filtered supernatants from stable pools were analyzed on an Octet R8 (Sartorius) using Protein A Biosensors (Sartorius) and yields of $sACE2_2$-IgG1 fusion proteins were similar between the pools. The top relative stable pool for each protein was progressed for protein production. The stable pools were adapted for one passage in CM76 media (Lonza Biologics) and production cultures in shake flasks were seeded with 0.2×10^6 cells/mL in CM125 media (Lonza Biologics). Bolus feeds were administered on days 4 and 8 consisting of a mixture of Lonza Biologics proprietary feeds. Production cultures were harvested on day 10 and sterile filtered using Sartoclear Dynamics Lab (Sartorius). Fusion proteins were purified using HiTrap MabSelect SuRe affinity chromatography (Cytiva). The column was equilibrated with 50 mM sodium phosphate pH 7.0, 125 mM NaCl, and washed with 50 mM sodium phosphate pH 7.0, 1 M NaCl, followed by a second wash with equilibration buffer. Proteins were eluted with 10 mM NaHCOO pH 3.5 and eluents were neutralized with 10× PBS, pH 7.4, and 1 M Tris-HCl pH 8.0. to pH ∼7.3. Eluted protein fractions were concentrated and separated on a Superdex 200 gel filtration column (Cytiva) as described above.

Capillary electrophoresis

Capillary electrophoresis-sodium dodecyl sulfate (CE-SDS) analysis was performed on an Agilent 2100 Bioanalyzer using the Agilent Protein 230 Kit (Agilent Technologies). Briefly, protein solutions were mixed 1:3 with denaturing solution with and without β-mercaptoethanol for reduced and non-reduced samples, respectively. Samples were heated to 95°C for 5 min, diluted 1:14 with water, and loaded onto a primed microfluidic chip for electrophoresis. Results were analyzed with 2100 Expert Software (Agilent Technologies).

Capillary isoelectric focusing electrophoresis (cIEF) was performed on a Maurice Capillary Electrophoresis (iCE) system (Bio-Techne). Samples were prepared at 0.2 mg/mL in sample buffer (0.35% methyl cellulose, 4% pharmalyte 3–10, 10 mM arginine) containing 4.05 and 9.99 pI markers. Running conditions were 1,500 V, 1 min, followed by 3,000 V, 4.5 min. Data were analyzed using Compass for iCE (Bio-Techne).

Sialic acid quantification

Sialic acids were released by acid hydrolysis (2 M acetic acid) of the test samples under heat and the α-keto functionality of the free sialic acids underwent a condensation reaction with 1,2-diamino-4,5-methylenedioxybenzene (DMB) to form fluorescent reaction products. Sialic acid standards were also labeled with DMB. Using RP-HPLC with fluorescence detection, N-acetylneuraminic acid (Neu5Ac) and N-glycolylneuraminic acid (Neu5Gc) were quantified.

Pseudovirus neutralization

Pseudovirus neutralization assays were contracted to GenScript ProBio. Briefly, pseudovirus with SARS-CoV-2 XBB.1.5 Spike was packaged in transfected HEK293T cells. Proteins were serially diluted 5-fold in Opti-MEM and added to an equal volume of pseudovirus solution. Mixed samples were incubated at room temperature for 1 h

and then added to a single-cell suspension of Opti-HEK293/ACE2 cells. Cells were cultured for 48 h and then processed with luciferase detection reagent. Relative luminescence units were measured on a plate reader and the data were analyzed using GraphPad Prism 6.0.

Purification of soluble HLA-II proteins

Soluble HLA-II heterodimers (DRB1*01:01, DRB1; DRB1*03:01, DRB3; DRB1*04:01, DRB4; DRB1*07:01, DRB7; DRB1*15:01, DRB15; DQB1*06:01/DQA1*01:02, DQB6; DPB1*02:01, DPB2; DPB1*04:01, DPB4) and HLA-DM were designed and purified similar to previously described methods.[78] Briefly, HLA-II allele constructs were cloned into a pcDNA3.1 expression plasmid with an N-terminal placeholder peptide[78] followed by a thrombin cleavage site, the HLA-II beta chain ectodomain C-terminally fused to a Jun leucine zipper helix, a StrepTagII epitope tag, and P2A ribosome skipping peptide. The P2A peptide was followed by the HLA-II alpha chain ectodomain fused to a Fos leucine zipper helix, and a C-terminal His-tag. HLA-II proteins were produced in Expi293F cells (Thermo Fisher) maintained in Expi293 Expression Medium (Thermo Fisher) and transiently transfected using the ExpiFectamine 293 Transfection Kit (Thermo Fisher) following the manufacturer's protocol. Purification was by NiNTA affinity capture, followed by buffer exchange and thrombin cleavage of the placeholder peptide prior to gel filtration to isolate HLA-II heterodimers. Proteins were concentrated and flash frozen in a final formulation of PBS with 16% glycerol.

Yeast display for HLA-II epitope immunogenicity assessment

EBY100 yeasts (ATCC) were transformed with a yeast display vector encoding an N-terminal Aga2p fusion with an HA epitope tag followed by a glycine-serine linker, a 17-amino acid ACE2 peptide centered on the site of mutation, a second glycine-serine linker sequence, and a C-terminal Myc-tag using a Frozen-EZ Yeast Transformation II Kit (Zymo Research) according to the manufacturer's instructions. For negative and positive controls, the ACE2 peptide sequence in the plasmid was replaced with polyserine or with peptide sequences that have high HLA-II affinity. Peptide sequences are listed in Table S14. Single colonies from -tryptophan/-uracil selection plates (Teknova) were transferred to 1 mL of SDCAA media (Teknova) and grown for ~24 h, 30°C, 225 rpm; 7.5×10^6 cells were collected, pelleted, and resuspended in 1 mL SGCAA media (Teknova) to induce Aga2p fusion peptide expression for 2 days at 30°C, 225 rpm. Yeasts were washed with PBS-BSA and resuspended in peptide exchange buffer (50 mM phosphate-citrate pH 5.0, 150 mM NaCl) at a density of ~50,000 cells/μL. Subsequently, 15 μL of yeast in exchange buffer were added to 15 μL of a solution containing purified HLA-II and HLA-DM in PBS with 16% glycerol to give final concentrations of 200 nM and 1 μM, respectively, and a final pH near 5.0. Samples were incubated at 37°C for 1 h with gentle shaking. Yeasts were pelleted and resuspended for 0.5 h with biotinylated anti-StrepTagII antibody (GenScript) in PBS-BSA at 4°C. Yeast were washed with PBS-BSA and stained with PE-conjugated streptavidin (Invitrogen) and Alexa Fluor 647-conjugated anti-Myc (Cell Signaling) for 0.5 h at 4°C. Prior to flow cytometry, cells were washed and resuspended in PBS-BSA for analysis. Change in mean fluorescence units (ΔMFU) plotted in Figure 5 are calculated from the mean PE fluorescence of the Myc-positive (i.e., peptide-expressing) yeast population minus the mean PE fluorescence of the Myc-negative population. Two negative controls were run in the experiments: "No HLA-II" controls included HLA-DM but not HLA-II protein, and a 15-amino acid polyserine peptide was used as a non-binding peptide control. Positive control peptides were previously verified as HLA-II binders by yeast display and/or by fluorescence polarization assays.

DATA AND CODE AVAILABILITY

All processed data supporting the findings of this study are available within the paper and its supplemental material. Unprocessed data are available from the corresponding authors upon reasonable request.

SUPPLEMENTAL INFORMATION

Supplemental information can be found online at https://doi.org/10.1016/j.omtm.2024.101301.

ACKNOWLEDGMENTS

Research reported in this publication was supported by the National Institutes of Health under Award Numbers R43AI162329 to K.K.C., R24GM137782 to P.A., and R01HL157489 and R01HL176493 to L.Z. This work was also supported in part by GlycoMIP, a National Science Foundation Materials Innovation Platform funded through Cooperative Agreement *DMR-1933525*. The content is solely the responsibility of the authors and does not necessarily represent the official views of the National Institutes of Health or National Science Foundation. Requests for materials belonging to Cyrus Biotechnology can be made to info@cyrusbio.com and will require a Material Transfer Agreement. The CHOK1SV GS-KO line requires a license from Lonza Biologics.

AUTHOR CONTRIBUTIONS

S.Skeeters screened mutant proteins, purified proteins, analyzed PK samples, and evaluated proteins by BLI, flow cytometry, and catalytic activity. K.B. and L.Z. performed BSL-3 experiments in the mouse COVID-19 model. G.S. purified proteins, analyzed PK samples, measured catalytic activity, and did flow cytometry. K.K.C. purified proteins and did BLI. B.D. developed PK analytics methods, tested PK samples, and did BLI. E.F. tested PK samples. D.T. and A.A. designed decoy receptors and predicted immunogenicity of variants with Y.S. supervising. L.B. developed the RD mutant. S.Shalygin, A.S., X.Y., and P.A. did glycomics and glycopeptidomics. D.T. coordinated with P.A. for initiating glycan analysis. K.A.B.-B. modeled PK. P.A.D. and M.M.S. tested peptide/HLA-II binding by yeast display. E.T. supervised PK analysis and coordinated representative manufacture in stable CHO pools with Lonza Biologics. E.P. supervised the overall program, coordinated PK studies with JAX, and drafted the original manuscript. JAX assisted with PK studies, GenScript ProBio assisted with pseudovirus neutralization, and Lonza Biologics assisted in production and analytics of proteins from stable CHOK1SV GS-KO pools. All authors were responsible for analyzing their respective data contributions.

DECLARATION OF INTERESTS

E.P. and L.Z. are inventors on a patent filing by the University of Illinois for ACE2 decoy receptors that is licensed to Cyrus Biotechnology. Employees of Cyrus Biotechnology are inventors on a patent filing covering optimized decoys for improved PK and hold stock and options.

REFERENCES

1. Ryu, G., and Shin, H.W. (2021). Sars-cov-2 infection of airway epithelial cells. Immune Netw. *21*, e3–e16. https://doi.org/10.4110/in.2021.21.e3.
2. Hoffmann, M., Kleine-Weber, H., Schroeder, S., Krüger, N., Herrler, T., Erichsen, S., Schiergens, T.S., Herrler, G., Wu, N.H., Nitsche, A., et al. (2020). SARS-CoV-2 Cell Entry Depends on ACE2 and TMPRSS2 and Is Blocked by a Clinically Proven Protease Inhibitor. Cell *181*, 271–280.e8. https://doi.org/10.1016/j.cell.2020.02.052.
3. Cantuti-Castelvetri, L., Ojha, R., Pedro, L.D., Djannatian, M., Franz, J., Kuivanen, S., van der Meer, F., Kallio, K., Kaya, T., Anastasina, M., et al. (2020). Neuropilin-1 facilitates SARS-CoV-2 cell entry and infectivity. Science *370*, 856–860. https://doi.org/10.1126/science.abd2985.
4. Dasgupta, C., and Zhang, L. (2011). Angiotensin II receptors and drug discovery in cardiovascular disease. Drug Discov. Today *16*, 22–34. https://doi.org/10.1016/j.drudis.2010.11.016.
5. Donoghue, M., Hsieh, F., Baronas, E., Godbout, K., Gosselin, M., Stagliano, N., Donovan, M., Woolf, B., Robison, K., Jeyaseelan, R., et al. (2000). A novel angiotensin-converting enzyme-related carboxypeptidase (ACE2) converts angiotensin I to angiotensin 1-9. Circ. Res. *87*, E1–E9. https://doi.org/10.1161/01.res.87.5.e1.
6. Vickers, C., Hales, P., Kaushik, V., Dick, L., Gavin, J., Tang, J., Godbout, K., Parsons, T., Baronas, E., Hsieh, F., et al. (2002). Hydrolysis of biological peptides by human angiotensin-converting enzyme-related carboxypeptidase. J. Biol. Chem. *277*, 14838–14843. https://doi.org/10.1074/jbc.M200581200.
7. Huang, Y., Yang, C., Xu, X.F., Xu, W., and Liu, S.W. (2020). Structural and functional properties of SARS-CoV-2 spike protein: potential antivirus drug development for COVID-19. Acta Pharmacol. Sin. *41*, 1141–1149. https://doi.org/10.1038/s41401-020-0485-4.
8. Hansen, J., Baum, A., Pascal, K.E., Russo, V., Giordano, S., Wloga, E., Fulton, B.O., Yan, Y., Koon, K., Patel, K., et al. (2020). Studies in humanized mice and convalescent humans yield a SARS-CoV-2 antibody cocktail. Science *369*, 1010–1014. https://doi.org/10.1126/science.abd0827.
9. Pinto, D., Sauer, M.M., Czudnochowski, N., Low, J.S., Alejandra Tortorici, M., Housley, M.P., Noack, J., Walls, A.C., Bowen, J.E., Guarino, B., et al. (2021). Broad betacoronavirus neutralization by a stem helix–specific human antibody. Science *373*, 1109–1116. https://doi.org/10.1126/science.abj3321.
10. Wec, A.Z., Wrapp, D., Herbert, A.S., Maurer, D.P., Haslwanter, D., Sakharkar, M., Jangra, R.K., Eugenia Dieterle, M., Lilov, A., Huang, D., et al. (2020). Broad neutralization of SARS-related viruses by human monoclonal antibodies. Science *369*, 731–736. https://doi.org/10.1126/science.abc7424.
11. Planas, D., Saunders, N., Maes, P., Guivel-Benhassine, F., Planchais, C., Buchrieser, J., Bolland, W.H., Porrot, F., Staropoli, I., Lemoine, F., et al. (2022). Considerable escape of SARS-CoV-2 Omicron to antibody neutralization. Nature *602*, 671–675. https://doi.org/10.1038/s41586-021-04389-z.
12. VanBlargan, L.A., Errico, J.M., Halfmann, P.J., Zost, S.J., Crowe, J.E., Purcell, L.A., Kawaoka, Y., Corti, D., Fremont, D.H., and Diamond, M.S. (2022). An infectious SARS-CoV-2 B.1.1.529 Omicron virus escapes neutralization by therapeutic monoclonal antibodies. Nat. Med. *28*, 490–495. https://doi.org/10.1038/s41591-021-01678-y.
13. Cao, Y., Yisimayi, A., Jian, F., Song, W., Xiao, T., Wang, L., Du, S., Wang, J., Li, Q., Chen, X., et al. (2022). BA.2.12.1, BA.4 and BA.5 escape antibodies elicited by Omicron infection. Nature *608*, 593–602. https://doi.org/10.1038/s41586-022-04980-y.
14. Cao, Y., Wang, J., Jian, F., Xiao, T., Song, W., Yisimayi, A., Huang, W., Li, Q., Wang, P., An, R., et al. (2022). Omicron escapes the majority of existing SARS-CoV-2 neutralizing antibodies. Nature *602*, 657–663. https://doi.org/10.1038/s41586-021-04385-3.
15. Zhang, L., Dutta, S., Xiong, S., Chan, M., Chan, K.K., Fan, T.M., Bailey, K.L., Lindeblad, M., Cooper, L.M., Rong, L., et al. (2022). Engineered ACE2 decoy mitigates lung injury and death induced by SARS-CoV-2 variants. Nat. Chem. Biol. *18*, 342–351. https://doi.org/10.1038/s41589-021-00965-6.
16. Viana, R., Moyo, S., Amoako, D.G., Tegally, H., Scheepers, C., Althaus, C.L., Anyaneji, U.J., Bester, P.A., Boni, M.F., Chand, M., et al. (2022). Rapid epidemic expansion of the SARS-CoV-2 Omicron variant in southern Africa. Nature *603*, 679–686. https://doi.org/10.1038/s41586-022-04411-y.
17. Tegally, H., Moir, M., Everatt, J., Giovanetti, M., Scheepers, C., Wilkinson, E., Subramoney, K., Makatini, Z., Moyo, S., Amoako, D.G., et al. (2022). Emergence of SARS-CoV-2 Omicron lineages BA.4 and BA.5 in South Africa. Nat. Med. *28*, 1785–1790. https://doi.org/10.1038/s41591-022-01911-2.
18. Callaway, E. (2022). COVID 'variant soup' is making winter surges hard to predict. Nature *611*, 213–214. https://doi.org/10.1038/d41586-022-03445-6.
19. Jing, W., and Procko, E. (2021). ACE2-based decoy receptors for SARS coronavirus 2. Proteins *89*, 1065–1078. https://doi.org/10.1002/prot.26140.
20. Song, R., Chen, X., Li, B., Zhang, H., Guo, X., Liu, Z., Zou, L., Liang, X., Lei, C., Mao, F., et al. (2023). Nasal spray of an IgM-like ACE2 fusion protein HH-120 accelerates SARS-CoV-2 clearance: A single-center propensity score-matched cohort study. J. Med. Virol. *95*, e28805. https://doi.org/10.1002/jmv.28805.
21. Song, R., Chen, X., Li, B., Ni, J., Zhou, Y., Zhang, H., Liang, X., Zou, L., Liu, J., Yang, F., et al. (2023). Nasal spray of an IgM-like ACE2 fusion protein HH-120 prevents SARS-CoV-2 infection: Two investigator-initiated postexposure prophylaxis trials. J. Med. Virol. *95*, e29275. https://doi.org/10.1002/jmv.29275.
22. Zoufaly, A., Poglitsch, M., Aberle, J.H., Hoepler, W., Seitz, T., Traugott, M., Grieb, A., Pawelka, E., Laferl, H., Wenisch, C., et al. (2020). Human recombinant soluble ACE2 in severe COVID-19. Lancet Respir. Med. *8*, 1154–1158. https://doi.org/10.1016/S2213-2600(20)30418-5.
23. Hettle, D., Hutchings, S., Muir, P., and Moran, E.; COVID-19 Genomics UK COG-UK consortium (2022). Persistent SARS-CoV-2 infection in immunocompromised patients facilitates rapid viral evolution: Retrospective cohort study and literature review. Clin. Infect. Pract. *16*, 100210. https://doi.org/10.1016/j.clinpr.2022.100210.
24. Dioverti, V., Salto-Alejandre, S., and Haidar, G. (2022). Immunocompromised Patients with Protracted COVID-19: a Review of "Long Persisters.". Curr. Transplant. Rep. *9*, 209–218. https://doi.org/10.1007/s40472-022-00385-y.
25. Chan, K.K., Dorosky, D., Sharma, P., Abbasi, S.A., Dye, J.M., Kranz, D.M., Herbert, A.S., and Procko, E. (2020). Engineering human ACE2 to optimize binding to the spike protein of SARS coronavirus 2. Science *369*, 1261–1265. https://doi.org/10.1126/SCIENCE.ABC0870.
26. Chan, K.K., Tan, T.J.C., Narayanan, K.K., and Procko, E. (2021). An engineered decoy receptor for SARS-CoV-2 broadly binds protein S sequence variants. Sci. Adv. *7*, eabf1738. https://doi.org/10.1126/sciadv.abf1738.
27. Zhang, L., Narayanan, K.K., Cooper, L., Chan, K.K., Skeeters, S.S., Devlin, C.A., Aguhob, A., Shirley, K., Rong, L., Rehman, J., et al. (2022). An ACE2 decoy can be administered by inhalation and potently targets omicron variants of SARS-CoV -2. EMBO Mol. Med. *14*, e16109. https://doi.org/10.15252/emmm.202216109.
28. Yamaguchi, T., Hoshizaki, M., Minato, T., Nirasawa, S., Asaka, M.N., Niiyama, M., Imai, M., Uda, A., Chan, J.F.W., Takahashi, S., et al. (2021). ACE2-like carboxypeptidase B38-CAP protects from SARS-CoV-2-induced lung injury. Nat. Commun. *12*, 6791. https://doi.org/10.1038/s41467-021-27097-8.
29. Kuba, K., Yamaguchi, T., and Penninger, J.M. (2021). Angiotensin-Converting Enzyme 2 (ACE2) in the Pathogenesis of ARDS in COVID-19. Front. Immunol. *12*, 732690. https://doi.org/10.3389/fimmu.2021.732690.
30. Imai, Y., Kuba, K., Rao, S., Huan, Y., Guo, F., Guan, B., Yang, P., Sarao, R., Wada, T., Leong-Poi, H., et al. (2005). Angiotensin-converting enzyme 2 protects from severe acute lung failure. Nature *436*, 112–116. https://doi.org/10.1038/nature03712.
31. Saunders, K.O. (2019). Conceptual approaches to modulating antibody effector functions and circulation half-life. Front. Immunol. *10*, 1296. https://doi.org/10.3389/fimmu.2019.01296.
32. Higuchi, Y., Suzuki, T., Arimori, T., Ikemura, N., Mihara, E., Kirita, Y., Ohgitani, E., Mazda, O., Motooka, D., Nakamura, S., et al. (2021). Engineered ACE2 receptor therapy overcomes mutational escape of SARS-CoV-2. Nat. Commun. *12*, 3802–3813. https://doi.org/10.1038/s41467-021-24013-y.

33. Liu, P., Xie, X., Gao, L., and Jin, J. (2020). Designed variants of ACE2-Fc that decouple anti-SARS-CoV-2 activities from unwanted cardiovascular effects. Int. J. Biol. Macromol. *165*, 1626–1633. https://doi.org/10.1016/j.ijbiomac.2020.10.120.

34. Iwanaga, N., Cooper, L., Rong, L., Maness, N.J., Beddingfield, B., Qin, Z., Crabtree, J., Tripp, R.A., Yang, H., Blair, R., et al. (2022). ACE2-IgG1 fusions with improved in vitro and in vivo activity against SARS-CoV-2. iScience *25*, 103670. https://doi.org/10.1016/j.isci.2021.103670.

35. Liu, P., Wysocki, J., Souma, T., Ye, M., Ramirez, V., Zhou, B., Wilsbacher, L.D., Quaggin, S.E., Batlle, D., and Jin, J. (2018). Novel ACE2-Fc chimeric fusion provides long-lasting hypertension control and organ protection in mouse models of systemic renin angiotensin system activation. Kidney Int. *94*, 114–125. https://doi.org/10.1016/j.kint.2018.01.029.

36. Lei, C., Qian, K., Li, T., Zhang, S., Fu, W., Ding, M., and Hu, S. (2020). Neutralization of SARS-CoV-2 spike pseudotyped virus by recombinant ACE2-Ig. Nat. Commun. *11*, 2070–2075. https://doi.org/10.1038/s41467-020-16048-4.

37. Proetzel, G., and Roopenian, D.C. (2014). Humanized FcRn mouse models for evaluating pharmacokinetics of human IgG antibodies. Methods *65*, 148–153. https://doi.org/10.1016/j.ymeth.2013.07.005.

38. Kenneth Hoober, J. (2020). Asgr1 and its enigmatic relative, CLEC10A. Int. J. Mol. Sci. *21*, 4818–4820. https://doi.org/10.3390/ijms21144818.

39. Yan, R., Zhang, Y., Li, Y., Xia, L., Guo, Y., and Zhou, Q. (2020). Structural basis for the recognition of SARS-CoV-2 by full-length human ACE2. Science *367*, 1444–1448. https://doi.org/10.1126/science.abb2762.

40. Li, F., Li, W., Farzan, M., and Harrison, S.C. (2005). Structural biology: Structure of SARS coronavirus spike receptor-binding domain complexed with receptor. Science *309*, 1864–1868. https://doi.org/10.1126/science.1116480.

41. Glasgow, A., Glasgow, J., Limonta, D., Solomon, P., Lui, I., Zhang, Y., Nix, M.A., Rettko, N.J., Zha, S., Yamin, R., et al. (2020). Engineered ACE2 receptor traps potently neutralize SARS-CoV-2. Proc. Natl. Acad. Sci. USA *117*, 28046–28055. https://doi.org/10.1073/pnas.2016093117.

42. Li, Y., Wang, H., Tang, X., Fang, S., Ma, D., Du, C., Wang, Y., Pan, H., Yao, W., Zhang, R., et al. (2020). SARS-CoV-2 and Three Related Coronaviruses Utilize Multiple ACE2 Orthologs and Are Potently Blocked by an Improved ACE2-Ig. J. Virol. *94*, e01283-20. https://doi.org/10.1128/jvi.01283-20.

43. Torchia, J.A., Tavares, A.H., Carstensen, L.S., Chen, D.Y., Huang, J., Xiao, T., Mukherjee, S., Reeves, P.M., Tu, H., Sluder, A.E., et al. (2022). Optimized ACE2 decoys neutralize antibody-resistant SARS-CoV-2 variants through functional receptor mimicry and treat infection in vivo. Sci. Adv. *8*, eabq6527. https://doi.org/10.1126/sciadv.abq6527.

44. Heurich, A., Hofmann-Winkler, H., Gierer, S., Liepold, T., Jahn, O., and Pöhlmann, S. (2014). TMPRSS2 and ADAM17 Cleave ACE2 Differentially and Only Proteolysis by TMPRSS2 Augments Entry Driven by the Severe Acute Respiratory Syndrome Coronavirus Spike Protein. J. Virol. *88*, 1293–1307. https://doi.org/10.1128/jvi.02202-13.

45. Liu, Y., Yang, Y., Zhang, C., Huang, F., Wang, F., Yuan, J., Wang, Z., Li, J., Li, J., Feng, C., et al. (2020). Clinical and biochemical indexes from 2019-nCoV infected patients linked to viral loads and lung injury. Sci. China Life Sci. *63*, 364–374. https://doi.org/10.1007/s11427-020-1643-8.

46. Kragstrup, T.W., Singh, H.S., Grundberg, I., Nielsen, A.L.L., Rivellese, F., Mehta, A., Goldberg, M.B., Filbin, M.R., Qvist, P., and Bibby, B.M. (2021). Plasma ACE2 predicts outcome of COVID-19 in hospitalized patients. PLoS One *16*, e0252799. https://doi.org/10.1371/journal.pone.0252799.

47. Lundström, A., Ziegler, L., Havervall, S., Rudberg, A., Meijenfeldt, F., Lisman, T., Mackman, N., Sandén, P., and Thålin, C. (2021). Soluble angiotensin-converting enzyme 2 is transiently elevated in COVID-19 and correlates with specific inflammatory and endothelial markers. J. Med. Virol. *93*, 5908–5916. https://doi.org/10.1002/jmv.27144.

48. Reindl-Schwaighofer, R., Hödlmoser, S., Eskandary, F., Poglitsch, M., Bonderman, D., Strassl, R., Aberle, J.H., Oberbauer, R., Zoufaly, A., and Hecking, M. (2021). ACE2 elevation in severe COVID-19. Am. J. Respir. Crit. Care Med. *203*, 1191–1196. https://doi.org/10.1164/rccm.202101-0142LE.

49. Fagyas, M., Fejes, Z., Sütő, R., Nagy, Z., Székely, B., Pócsi, M., Ivády, G., Bíró, E., Bekő, G., Nagy, A., et al. (2022). Circulating ACE2 activity predicts mortality and disease severity in hospitalized COVID-19 patients. Int. J. Infect. Dis. *115*, 8–16. https://doi.org/10.1016/j.ijid.2021.11.028.

50. Carpenter, R.M., Young, M.K., Petri, W.A.O., Lyons, G.R., Gilchrist, C., Carey, R.M., and Petri, W.A. (2022). Repressed Ang 1–7 in COVID-19 Is Inversely Associated with Inflammation and Coagulation. mSphere *7*, e0022022. https://doi.org/10.1128/msphere.00220-22.

51. Daniell, H., Nair, S.K., Shi, Y., Wang, P., Montone, K.T., Shaw, P.A., Choi, G.H., Ghani, D., Weaver, J.E., Rader, D.J., et al. (2022). Decrease in Angiotensin-Converting Enzyme activity but not concentration in plasma/lungs in COVID-19 patients offers clues for diagnosis/treatment. Mol. Ther. Methods Clin. Dev. *26*, 266–278. https://doi.org/10.1016/j.omtm.2022.07.003.

52. Leman, J.K., Weitzner, B.D., Lewis, S.M., Adolf-Bryfogle, J., Alam, N., Alford, R.F., Aprahamian, M., Baker, D., Barlow, K.A., Barth, P., et al. (2020). Macromolecular modeling and design in Rosetta: recent methods and frameworks. Nat. Methods *17*, 665–680. https://doi.org/10.1038/s41592-020-0848-2.

53. Shajahan, A., Archer-Hartmann, S., Supekar, N.T., Gleinich, A.S., Heiss, C., and Azadi, P. (2021). Comprehensive characterization of N-and O-glycosylation of SARS-CoV-2 human receptor angiotensin converting enzyme 2. Glycobiology *31*, 410–424. https://doi.org/10.1093/glycob/cwaa101.

54. Kuba, K., Imai, Y., Rao, S., Gao, H., Guo, F., Guan, B., Huan, Y., Yang, P., Zhang, Y., Deng, W., et al. (2005). A crucial role of angiotensin converting enzyme 2 (ACE2) in SARS coronavirus-induced lung injury. Nat. Med. *11*, 875–879. https://doi.org/10.1038/nm1267.

55. Robbie, G.J., Criste, R., Dall'Acqua, W.F., Jensen, K., Patel, N.K., Losonsky, G.A., and Griffin, M.P. (2013). A novel investigational Fc-modified humanized monoclonal antibody, motavizumab-YTE, has an extended half-life in healthy adults. Antimicrob. Agents Chemother. *57*, 6147–6153. https://doi.org/10.1128/AAC.01285-13.

56. Acqua, W.F.D., Woods, R.M., Ward, E.S., Palaszynski, S.R., Patel, N.K., Brewah, Y.A., Wu, H., Kiener, P.A., and Langermann, S. (2002). Increasing the Affinity of a Human IgG1 for the Neonatal Fc Receptor: Biological Consequences. J. Immunol. *169*, 5171–5180. https://doi.org/10.4049/jimmunol.169.9.5171.

57. Dall'Acqua, W.F., Kiener, P.A., and Wu, H. (2006). Properties of Human IgG1s engineered for enhanced binding to the neonatal Fc Receptor (FcRn). J. Biol. Chem. *281*, 23514–23524. https://doi.org/10.1074/jbc.M604292200.

58. Loo, Y.M., McTamney, P.M., Arends, R.H., Abram, M.E., Aksyuk, A.A., Diallo, S., Flores, D.J., Kelly, E.J., Ren, K., Roque, R., et al. (2022). The SARS-CoV-2 monoclonal antibody combination, AZD7442, is protective in nonhuman primates and has an extended half-life in humans. Sci. Transl. Med. *14*, eabl8124. https://doi.org/10.1126/scitranslmed.abl8124.

59. Moore, M.J., Dorfman, T., Li, W., Wong, S.K., Li, Y., Kuhn, J.H., Coderre, J., Vasilieva, N., Han, Z., Greenough, T.C., et al. (2004). Retroviruses Pseudotyped with the Severe Acute Respiratory Syndrome Coronavirus Spike Protein Efficiently Infect Cells Expressing Angiotensin-Converting Enzyme 2. J. Virol. *78*, 10628–10635. https://doi.org/10.1128/jvi.78.19.10628-10635.2004.

60. Tripathi, N.K., and Shrivastava, A. (2019). Recent Developments in Bioprocessing of Recombinant Proteins: Expression Hosts and Process Development. Front. Bioeng. Biotechnol. *7*, 420. https://doi.org/10.3389/fbioe.2019.00420.

61. Fan, L., Kadura, I., Krebs, L.E., Hatfield, C.C., Shaw, M.M., and Frye, C.C. (2012). Improving the efficiency of CHO cell line generation using glutamine synthetase gene knockout cells. Biotechnol. Bioeng. *109*, 1007–1015. https://doi.org/10.1002/bit.24365.

62. Feary, M., Racher, A.J., Young, R.J., and Smales, C.M. (2017). Methionine sulfoximine supplementation enhances productivity in GS–CHOK1SV cell lines through glutathione biosynthesis. Biotechnol. Prog. *33*, 17–25. https://doi.org/10.1002/btpr.2372.

63. Li, X., Burnight, E.R., Cooney, A.L., Malani, N., Brady, T., Sander, J.D., Staber, J., Wheelan, S.J., Joung, J.K., McCray, P.B., et al. (2013). PiggyBac transposase tools for genome engineering. Proc. Natl. Acad. Sci. USA *110*, E2279–E2287. https://doi.org/10.1073/pnas.1305987110.

64. Flintegaard, T.V., Thygesen, P., Rahbek-Nielsen, H., Levery, S.B., Kristensen, C., Clausen, H., and Bolt, G. (2010). N-glycosylation increases the circulatory half-life

of human growth hormone. Endocrinology *151*, 5326–5336. https://doi.org/10.1210/en.2010-0574.

65. Mastrangeli, R., Audino, M.C., Palinsky, W., Broly, H., and Bierau, H. (2021). Current views on N-glycolylneuraminic acid in therapeutic recombinant proteins. Trends Pharmacol. Sci. *42*, 943–956. https://doi.org/10.1016/j.tips.2021.08.004.

66. Jafari, R., Zolbanin, N.M., Rafatpanah, H., Majidi, J., and Kazemi, T. (2017). Fc-fusion Proteins in Therapy: An Updated View. Curr. Med. Chem. *24*, 1228–1237. https://doi.org/10.2174/0929867324666170113112759.

67. Khan, A., Benthin, C., Zeno, B., Albertson, T.E., Boyd, J., Christie, J.D., Hall, R., Poirier, G., Ronco, J.J., Tidswell, M., et al. (2017). A pilot clinical trial of recombinant human angiotensin-converting enzyme 2 in acute respiratory distress syndrome. Crit. Care *21*, 234. https://doi.org/10.1186/s13054-017-1823-x.

68. Haschke, M., Schuster, M., Poglitsch, M., Loibner, H., Salzberg, M., Bruggisser, M., Penninger, J., and Krähenbühl, S. (2013). Pharmacokinetics and pharmacodynamics of recombinant human angiotensin-converting enzyme 2 in healthy human subjects. Clin. Pharmacokinet. *52*, 783–792. https://doi.org/10.1007/s40262-013-0072-7.

69. Simon, M.A., Hanrott, K., Budd, D.C., Torres, F., Grünig, E., Escribano-Subias, P., Meseguer, M.L., Halank, M., Opitz, C., Hall, D.A., et al. (2022). An open-label, dose-escalation study to evaluate the safety, tolerability, pharmacokinetics, and pharmacodynamics of single doses of GSK2586881 in participants with pulmonary arterial hypertension. Pulm. Circ. *12*, e12024. https://doi.org/10.1002/pul2.12024.

70. Hall, D.A., Hanrott, K., Badorrek, P., Berliner, D., Budd, D.C., Eames, R., Powley, W.M., Hewens, D., Siederer, S., Lazaar, A.L., et al. (2021). Effects of Recombinant Human Angiotensin-Converting Enzyme 2 on Response to Acute Hypoxia and Exercise: A Randomised, Placebo-Controlled Study. Pulm. Ther. *7*, 487–501. https://doi.org/10.1007/s41030-021-00164-7.

71. Karle, A.C. (2020). Applying MAPPs Assays to Assess Drug Immunogenicity. Front. Immunol. *11*, 698. https://doi.org/10.3389/fimmu.2020.00698.

72. Paul, S., Kolla, R.V., Sidney, J., Weiskopf, D., Fleri, W., Kim, Y., Peters, B., and Sette, A. (2013). Evaluating the immunogenicity of protein drugs by applying in vitro MHC binding data and the immune epitope database and analysis resource. Clin. Dev. Immunol. *2013*, 467852. https://doi.org/10.1155/2013/467852.

73. King, C., Garza, E.N., Mazor, R., Linehan, J.L., Pastan, I., Pepper, M., and Baker, D. (2014). Removing T-cell epitopes with computational protein design. Proc. Natl. Acad. Sci. USA *111*, 8577–8582. https://doi.org/10.1073/pnas.1321126111.

74. Gragert, L., Madbouly, A., Freeman, J., and Maiers, M. (2013). Six-locus high resolution HLA haplotype frequencies derived from mixed-resolution DNA typing for the entire US donor registry. Hum. Immunol. *74*, 1313–1320. https://doi.org/10.1016/j.humimm.2013.06.025.

75. Hollenbach, J.A., Madbouly, A., Gragert, L., Vierra-Green, C., Flesch, S., Spellman, S., Begovich, A., Noreen, H., Trachtenberg, E., Williams, T., et al. (2012). A combined DPA1∼DPB1 amino acid epitope is the primary unit of selection on the HLA-DP heterodimer. Immunogenetics *64*, 559–569. https://doi.org/10.1007/s00251-012-0615-3.

76. Klitz, W., Maiers, M., Spellman, S., Baxter-Lowe, L.A., Schmeckpeper, B., Williams, T.M., and Fernandez-Viña, M. (2003). New HLA haplotype frequency reference standards: High-resolution and large sample typing of HLA DR-DQ haplotypes in a sample of European Americans. Tissue Antigens *62*, 296–307. https://doi.org/10.1034/j.1399-0039.2003.00103.x.

77. Jones, E.Y., Fugger, L., Strominger, J.L., and Siebold, C. (2006). MHC class II proteins and disease: A structural perspective. Nat. Rev. Immunol. *6*, 271–282. https://doi.org/10.1038/nri1805.

78. Vyasamneni, R., Kohler, V., Karki, B., Mahimkar, G., Esaulova, E., McGee, J., Kallin, D., Sheen, J.H., Harjanto, D., Kirsch, M., et al. (2023). A universal MHCII technology platform to characterize antigen-specific CD4+ T cells. Cell Rep. Methods *3*, 100388. https://doi.org/10.1016/j.crmeth.2022.100388.

79. Huisman, B.D., Balivada, P.A., and Birnbaum, M.E. (2023). Yeast display platform with expression of linear peptide epitopes for high-throughput assessment of peptide-MHC-II binding. J. Biol. Chem. *299*, 102913. https://doi.org/10.1016/j.jbc.2023.102913.

80. Benjakul, S., Anthi, A.K., Kolderup, A., Vaysburd, M., Lode, H.E., Mallery, D., Fossum, E., Vikse, E.L., Albecka, A., Ianevski, A., et al. (2023). A pan-SARS-CoV-2-specific soluble angiotensin-converting enzyme 2-albumin fusion engineered for enhanced plasma half-life and needle-free mucosal delivery. PNAS Nexus *2*, pgad403. https://doi.org/10.1093/pnasnexus/pgad403.

81. Zhou, Q., and Qiu, H. (2019). The Mechanistic Impact of N-Glycosylation on Stability, Pharmacokinetics, and Immunogenicity of Therapeutic Proteins. J. Pharm. Sci. *108*, 1366–1377. https://doi.org/10.1016/j.xphs.2018.11.029.

82. Chia, S., Tay, S.J., Song, Z., Yang, Y., Walsh, I., and Pang, K.T. (2023). Enhancing pharmacokinetic and pharmacodynamic properties of recombinant therapeutic proteins by manipulation of sialic acid content. Biomed. Pharmacother. *163*, 114757. https://doi.org/10.1016/j.biopha.2023.114757.

83. Morell, A.G., Gregoriadis, G., Scheinberg, I.H., Hickman, J., and Ashwell, G. (1971). The role of sialic acid in determining the survival of glycoproteins in the circulation. J. Biol. Chem. *246*, 1461–1467. https://doi.org/10.1016/s0021-9258(19)76994-4.

84. Liu, L., Gomathinayagam, S., Hamuro, L., Prueksaritanont, T., Wang, W., Stadheim, T.A., and Hamilton, S.R. (2013). The impact of glycosylation on the pharmacokinetics of a TNFR2:Fc fusion protein expressed in glycoengineered pichia pastoris. Pharm. Res. (N. Y.) *30*, 803–812. https://doi.org/10.1007/s11095-012-0921-3.

85. Capraz, T., Kienzl, N.F., Laurent, E., Perthold, J.W., Höbenreich, E.F., Grünwald-Gruber, C., Maresch, D., Monteil, V., Niederhöfer, J., Wirnsberger, G., et al. (2021). Structure-guided glyco-engineering of ACE2 for improved potency as soluble SARS-CoV-2 decoy receptor. Elife *10*, e73641. https://doi.org/10.7554/eLife.73641.

86. Izadi, S., Vavra, U., Melnik, S., Grünwald-Gruber, C., Föderl-Höbenreich, E., Sack, M., Zatloukal, K., Glössl, J., Stöger, E., Mach, L., et al. (2023). In planta deglycosylation improves the SARS-CoV-2 neutralization activity of recombinant ACE2-Fc. Front. Bioeng. Biotechnol. *11*, 1180044. https://doi.org/10.3389/fbioe.2023.1180044.

87. Castilho, A., Schwestka, J., Kienzl, N.F., Vavra, U., Grünwald-Gruber, C., Izadi, S., Hiremath, C., Niederhöfer, J., Laurent, E., Monteil, V., et al. (2021). Generation of enzymatically competent SARS-CoV-2 decoy receptor ACE2-Fc in glycoengineered Nicotiana benthamiana. Biotechnol. J. *16*, e2000566. https://doi.org/10.1002/biot.202000566.

88. Ducret, A., Ackaert, C., Bessa, J., Bunce, C., Hickling, T., Jawa, V., Kroenke, M.A., Lamberth, K., Manin, A., Penny, H.L., et al. (2022). Assay format diversity in preclinical immunogenicity risk assessment: Toward a possible harmonization of antigenicity assays. mAbs *14*, 1993522. https://doi.org/10.1080/19420862.2021.1993522.

89. Lebedin, M., García, C.V., Spatt, L., Ratswohl, C., Thibeault, C., Ostendorf, L., Alexander, T., Paul, F., Sander, L.E., Kurth, F., et al. (2023). Discriminating promiscuous from target-specific autoantibodies in COVID-19. Eur. J. Immunol. *53*, e2250210. https://doi.org/10.1002/eji.202250210.

90. Muri, J., Cecchinato, V., Cavalli, A., Shanbhag, A.A., Matkovic, M., Biggiogero, M., Maida, P.A., Moritz, J., Toscano, C., Ghovehoud, E., et al. (2023). Autoantibodies against chemokines post-SARS-CoV-2 infection correlate with disease course. Nat. Immunol. *24*, 604–611. https://doi.org/10.1038/s41590-023-01445-w.

91. Bastard, P., Rosen, L.B., Zhang, Q., Michailidis, E., Hoffmann, H.H., Zhang, Y., Dorgham, K., Philippot, Q., Rosain, J., Béziat, V., et al. (2020). Autoantibodies against type I IFNs in patients with life-threatening COVID-19. Science *370*, eabd4585. https://doi.org/10.1126/science.abd4585.

92. Chang, S.E., Feng, A., Meng, W., Apostolidis, S.A., Mack, E., Artandi, M., Barman, L., Bennett, K., Chakraborty, S., Chang, I., et al. (2021). New-onset IgG autoantibodies in hospitalized patients with COVID-19. Nat. Commun. *12*, 5417. https://doi.org/10.1038/s41467-021-25509-3.

93. Woodruff, M.C., Ramonell, R.P., Haddad, N.S., Anam, F.A., Rudolph, M.E., Walker, T.A., Truong, A.D., Dixit, A.N., Han, J.E., Cabrera-Mora, M., et al. (2022). Dysregulated naive B cells and de novo autoreactivity in severe COVID-19. Nature *611*, 139–147. https://doi.org/10.1038/s41586-022-05273-0.

94. Monteil, V., Kwon, H., Prado, P., Hagelkrüys, A., Wimmer, R.A., Stahl, M., Leopoldi, A., Garreta, E., Hurtado del Pozo, C., Prosper, F., et al. (2020). Inhibition of SARS-CoV-2 Infections in Engineered Human Tissues Using Clinical-Grade Soluble Human ACE2. Cell *181*, 905–913.e7. https://doi.org/10.1016/j.cell.2020.04.004.

95. Monteil, V., Eaton, B., Postnikova, E., Murphy, M., Braunsfeld, B., Crozier, I., Kricek, F., Niederhöfer, J., Schwarzböck, A., Breid, H., et al. (2022). Clinical grade

ACE2 as a universal agent to block SARS-CoV -2 variants. EMBO Mol. Med. *14*, e15230. https://doi.org/10.15252/emmm.202115230.

96. Ma, J., Lee, K.V., and Stafford, R.S. (2006). Changes in antihypertensive prescribing during US outpatient visits for uncomplicated hypertension between 1993 and 2004. Hypertension *48*, 846–852. https://doi.org/10.1161/01.HYP.0000240931.90917.0c.

97. Takuathung, M.N., Sakuludomkan, W., Khatsri, R., Dukaew, N., Kraivisitkul, N., Ahmadmusa, B., Mahakkanukrauh, C., Wangthaweesap, K., Onin, J., Srichai, S., et al. (2022). Adverse Effects of Angiotensin-Converting Enzyme Inhibitors in Humans: A Systematic Review and Meta-Analysis of 378 Randomized Controlled Trials. Int. J. Environ. Res. Public Health *19*, 8373. https://doi.org/10.3390/ijerph19148373.

98. Vítovec, J., and Špinar, J. (2000). First-dose hypotension after angiotensin-converting enzyme (ACE) inhibitors in chronic heart failure: a comparison of enalapril and perindopril. Slovak Investigator Group. Eur. J. Heart Fail. *2*, 299–304. https://doi.org/10.1016/S1388-9842(00)00095-7.

99. Goyal, A., Cusick, A.S., and Thielemier, B. (2024). ACE Inhibitors (StatPearls Publishing).

100. Frenz, B., Lewis, S.M., King, I., DiMaio, F., Park, H., and Song, Y. (2020). Prediction of Protein Mutational Free Energy: Benchmark and Sampling Improvements Increase Classification Accuracy. Front. Bioeng. Biotechnol. *8*, 558247. https://doi.org/10.3389/fbioe.2020.558247.

101. Bhardwaj, G., Mulligan, V.K., Bahl, C.D., Gilmore, J.M., Harvey, P.J., Cheneval, O., Buchko, G.W., Pulavarti, S.V.S.R.K., Kaas, Q., Eletsky, A., et al. (2016). Accurate de novo design of hyperstable constrained peptides. Nature *538*, 329–335. https://doi.org/10.1038/nature19791.

102. Wang, W., and Prueksaritanont, T. (2010). Prediction of human clearance of therapeutic proteins: Simple allometric scaling method revisited. Biopharm. Drug Dispos. *31*, 253–263. https://doi.org/10.1002/bdd.708.

103. Betts, A., Keunecke, A., van Steeg, T.J., van der Graaf, P.H., Avery, L.B., Jones, H., and Berkhout, J. (2018). Linear pharmacokinetic parameters for monoclonal antibodies are similar within a species and across different pharmacological targets: A comparison between human, cynomolgus monkey and hFcRn Tg32 transgenic mouse using a population-modeling approach. mAbs *10*, 751–764. https://doi.org/10.1080/19420862.2018.1462429.